

When the Hubble Sequence Appeared?: Morphology, Color, and Number-Density Evolution of the Galaxies in the Hubble Deep Field North.

Masaru KAJISAWA

and

Toru YAMADA

National Astronomical Observatory, 2-21-1, Osawa, Mitaka, Tokyo 181-8588

E-mail(MK): kajisawa@optik.mtk.nao.ac.jp

(Received ; accepted)

Abstract

Using the HST WFPC2/NICMOS archival data of the Hubble Deep Field North, we construct the nearly complete sample of the $M_V < -20$ ($\sim L^* + 1$) galaxies to $z = 2$, and investigate when the Hubble sequence appeared, namely, the evolution of the morphology, colors, and the comoving number density of the sample. Even if taking into account of the uncertainty of the photometric redshift technique, the number density of relatively bright bulge-dominated galaxies in the HDF-N decrease significantly at $z > 1$, and their rest-frame $U - V$ color distribution is wide-spread over $0.5 < z < 2$. On the other hand, while the number density of both disk-dominated and irregular galaxies does not show significant change at $z < 2$, their distribution of the rest-frame $U - V$ color alters at $z \sim 1.5$: there is no relatively red (rest $U - V \gtrsim 0.3$) galaxies at $z > 1.5$, while the significant fraction of these red disk-dominated or irregular galaxies exists at $z < 1.5$. These results suggest that the significant evolution of the Hubble sequence which is seen in the present Universe occurs at $1 < z < 2$.

Key words: Galaxies: field — Galaxies: evolution — Galaxies:formation

1. Introduction

Since Hubble (1926; 1936), galaxy properties are known to be broadly classified along the sequence of their morphology, namely, bulge-to-disk luminosity ratio and the tightness of the spiral arm structure, from ellipticals (E) to irregular (Irr) galaxies. The classification has been repeatedly tested and expanded (e.g., de Vaucouleurs 1959; Sandage 1975; Buta 1992 a,b; Roberts and Haynes 1994; see Abraham 1999 for the recent review). Along the Hubble sequence, some physical properties of the galaxies changes. The cold gas to luminous mass ratio changes systematically from Scd to E type (Roberts and Haynes 1994), and thus the sequence must represent the different evolutionary history of the galaxies. Consequently, the colors and spectral properties also change along the Hubble sequence. In fact, local galaxies are known to lie on a sequence in $U - V$ and $B - V$ two color diagram (Huchra 1977; Kennicutt 1983). In other words, galaxy SED can be characterized by the rest-frame $U - V$ color since this color is sensitive to the existence/absence of the largest features in galaxy continuum spectra at near-UV to optical wavelength, namely, 4000 Å break or the Balmer discontinuity that represent the average age and/or metallicity of the stellar population in the galaxies.

Thanks to the recent developments of technology, photometric properties of galaxies can be traced toward very high redshift and the evolution of the Hubble sequence can be directly and empirically tested. It is very exciting to observe when and how the Hubble sequence appeared as we see in the local universe.

The combinations of redshift survey and high resolution imaging with Hubble Space Telescope (HST) have revealed that the large, normal galaxies such as those represented in the Hubble sequence scheme show little or mild evolution to $z \sim 1$ (e.g., Schade et al. 1996; Brinchmann et al. 1998; Lilly et al. 1998). On the other hand, the large sample of star-forming galaxies at $z > 3$ was discovered with ‘drop-out’ technique (e.g., Steidel et al. 1996; 1999) and these Lyman Break Galaxies are found to have the morphology that is clearly different from Hubble sequence not only in the rest-frame UV wavelength but also in the rest-frame optical region (Dickinson 2000a).

From these previous studies, therefore, the intermediate redshift range at $1 < z < 2$ is supposed to be very important era for the formation of the Hubble sequence.

However, there are some difficulties in studying a well defined sample of galaxies at $1 < z < 2$. Firstly, the optical flux-limited selection of galaxies is biased to detect more blue star-forming galaxies at $z \gtrsim 1.3$ since it samples the rest-frame UV-luminous objects in the redshift range. In order to study the evolution of Hubble sequence, the sample should contains quiescent galaxies as the local early-type objects. Sample selection in NIR wavelength is essential to construct a nearly mass-limited sample to study the evolution of colors, morphologies, and the number density of the galaxies in certain mass range. Limited area of the infrared detectors and the high background sky noise in the ground-base observations, however, generally prevent us from building an ideal sample of galaxies in the redshift range with fairly large volume and depth.

It is also difficult to identify the redshift of galaxies in this range by optical spectroscopy since the major emission lines and continuum breaks get out of optical wavelength. The depth and multiplicity in NIR spectroscopy is still much limited compared to the optical ones. Alternative way of determining the redshift of galaxies at $1 < z < 2$ is that by photometric redshift technique with multi-band optical-NIR photometric data.

Further, galaxy morphology appears differently when seen in the different wavelength. At high redshift, the morphological K-correction (e.g., O’Connell 1997) seems to be significant in the optical images, particularly for disk galaxies. NIR high-resolution image that can allow the morphological classification for galaxies at $z > 1$ is needed to overcome this problem.

In this paper, in order to understand the formation and evolution of the Hubble sequence, we construct the nearly complete sample of the $M_V < -20$ ($\sim L^* + 1$) galaxies in the HDF-N to $z = 2$ using the archival HST/NICMOS NIR data in addition to the optical WFPC2 data. We investigate the changes of the distributions of galaxy morphology, luminosity and colors since $z = 2$ with this sample. Thanks to the deep NICMOS images, we can sample galaxies at $1 < z < 2$ to $M_V < -20$ with very high completeness, and the high resolution of these images also enable us to examine the galaxy morphology in the same rest-frame wavelength at each redshift.

It is known that galaxy morphological fraction changes with the absolute magnitude range (Binggelli, Sandage, and Tammann 1988; Marzke et al. 1994; van den Bergh 1997). Marzke et al. obtained the fitted L_* values of the luminosity function for each type of the galaxies as -20.7 for E and $\approx -20.2 - 3$ for S0 to Sm-Im ($H_0 = 50 \text{ km s}^{-1} \text{ Mpc}^{-1}$). According to the van den Bergh (1997) who reviewed the Revised Shapley Ames Catalog for Bright Galaxies (RSA2, Sandage and Tammann 1987), more than 90% of the galaxies with E-Sb and 80% of the galaxies with Sc in the RSA2 catalog have absolute magnitude of $M_V < -20$ though only a 20% of the galaxies later than Scd in RSA2 are found in the luminosity range. Although there is some uncertainty for the luminosity function of the galaxies later than Scd, the limit of $M_V < -20$, as the baseline, provides us to recover the Hubble sequence from E to at least Sc type *in the local universe*.

On the other hand, we also suffer the small volume effect in the current analysis since the HDF-N covers at most $\sim 4 \text{ arcmin}^2$. It should be reminded that the results obtained from such a small field could be easily affected by large-scale structure. However, the WFPC2 + NICMOS data of the HDF-N are the wide wavelength coverage, highest resolution, deepest images at the present, and provide us the nearly the first opportunity to obtain the implication for the understanding of the formation of the Hubble sequence. Note that the region also samples the comoving depth of 1.9 Gpc between $1 < z < 2$ although only $\sim 10^4 \text{ Mpc}^{-3}$ in comoving volume ($H_0 = 70 \text{ km s}^{-1} \text{ Mpc}^{-1}$, $\Omega_0 = 0.3$, $\Omega_\Lambda = 0.7$).

Dickinson (2000b) originally studied the same HST WFPC2/NICMOS data of the HDF-N, and investigated the morphology, luminosity, color, number density of relatively bright $z < 2$ galaxies with similar luminosity range to those studied here. They found the similarity between the rest UV and optical

morphology of irregular galaxies, the existence of the large, ordinary spiral galaxies to $z \sim 1.2$ and the red giant ellipticals to $z \sim 1.8$, the presence of bluer early-type galaxies at $0.5 < z < 1.4$, and the deficit of bright galaxies at $z > 1$ in all morphological types.

For the morphologically-selected galaxies, Franceschini et al.(1998) and Rodighiero et al.(2000) also investigated the redshift distribution of the galaxies in the HDF-N and found the deficit of bright objects at $z \gtrsim 1.3$ in each morphology.

In this paper, we also tested these results by our own morphological classification, color analysis in the different wavelength, taking into the various uncertainties in the sample selection due to the cosmology, photometric redshift procedure, and band-shifting effect.

In section 2, we describe the data reduction, and the selection procedure of our sample. We investigate the evolution of number density and color distribution of these galaxies, and check these results, especially about the uncertainty of the photometric redshift estimate in section 3. The discussion about these results is presented in section 4, and we summarize our conclusion in the final section. We use AB magnitude system (Oke 1974) for HST filter bands, and refer F300W, F450W, F606W, F814W, F110W, F160W bands as U_{300} , B_{450} , V_{606} , I_{814} , J_{110} , H_{160} , respectively, through the paper.

2. Data Reduction & Sample Selection

2.1. HST WFPC2/NICMOS data

The HDF-N is observed with HST NICMOS Camera 3 between UT 1998 June 13 and June 23 (PI:M. Dickinson; PID 7817). The complete HDF-N was mosaiced with eight sub fields in J_{110} and H_{160} -bands. We analyzed the calibrated data of these observations downloaded from the archival site of the Space Telescope Science Institute. Each sub field was observed through the nine dithered pointings, with a net exposure of 12600 sec in each band, except for a few pointings that cannot be used due to guidance error of HST (Dickinson et al. 2000). We combine these data into a single mosaiced image registered to WFPC2 image of HDF-N, using the ‘‘drizzling’’ method with *IRAF DITHER* package. The FWHM of the final drizzled image is about 0.22 arcsec.

For optical data, we analyzed the public ‘‘version 2’’ U_{300} , B_{450} , V_{606} , I_{814} -band WFPC2 images of HDF-N produced by the STScI team. The optical images were convolved with Gaussian kernel to match the NICMOS point spread function.

2.2. Source Detection & Photometry

At first, we performed source detection in the H_{160} -band image using the SExtractor image analysis package (Bertin & Arnouts 1996). A detection threshold of $\mu_H = 25.5$ mag arcsec² over 15 connected pixels was used. We adopt MAG_BEST from SExtractor as total magnitude of each detected object. Of the sources extracted by SExtractor, objects located at the edge of WFPC2 frames and those, which we

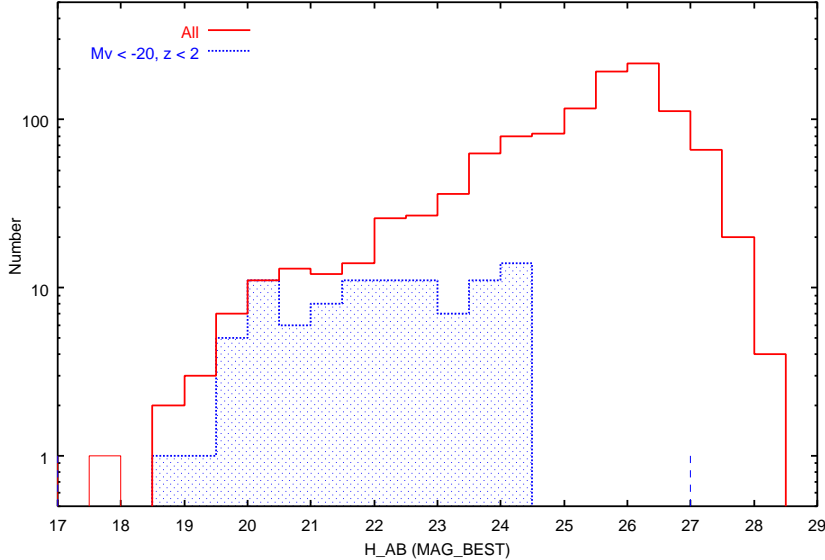


Fig. 1.. Raw H_{110} -band number counts of the Hubble Deep Field North (solid line). Dotted line shows the galaxies with $M_V < -20$ at $z < 2$.

identified by eyes as noise peaks (mostly near the bright objects) are rejected and removed from the final catalog.

Figure 1 shows the raw number counts of H_{160} -band frame. From the figure, we infer that the object detection is nearly complete to $H_{160} = 25.5-26.0$. In fact, the sensitivity of the frame varies over the field of view due to variations in exposure time and NICMOS quantum efficiency (Dickinson et al. 2000). But this does not provide important effect in our analysis later on, since we concentrate on the objects at least 1-1.5 mag brighter than above completeness limit in this paper (see next subsection).

We cataloged the objects with $H_{160} < 26$, and performed the photometry with $1.2''$ diameter aperture for the all six U_{300} , B_{450} , V_{606} , I_{814} , J_{110} , H_{160} -band images. The aperture position for each object is fixed in order to measure the colors or broad band SED at the same physical region of the galaxy. 631 objects were cataloged and their magnitude was measured.

2.3. Redshift determination & Sample Selection

Cohen et al.(2000) compiled the HDF galaxies with the redshifts confirmed by spectroscopy so far. We identified the corresponding objects in our $H_{160} < 26$ catalogue, by comparing the coordinates of the objects in Cohen et al.'s catalogue and ours. 139 out of 631 objects were identified and the spectroscopic redshifts of Cohen et al. can be used. Cohen et al's sample was selected mainly by standard $R \leq 24$ mag, and limited to $z \lesssim 1.3$ except for the Lyman Break Galaxies at $z > 2$ (e.g, Lowenthal et al 1997,

Dickinson 1998).

For the objects with no spectroscopic redshift, we can estimate their redshifts by using photometric redshift technique with the photometric data of the six optical-NIR bands mentioned in previous subsection. We computed photometric redshifts of those objects by using the public code of *hyperz* (Bolzonella et al. 2000). The photometric redshift is calculated by χ^2 minimization, comparing the observed magnitudes to the values expected from a set of model Spectral Energy Distribution. The free parameters involved in the fitting are the redshift, spectral type (star formation history), age, color excess (dust extinction). We chose to use the SED model of Bruzual & Charlot synthetic library (GISSEL98, Bruzual & Charlot 1993) and the Calzetti extinction law (Calzetti et al. 2000). We excluded the stars that confirmed by spectroscopy from our sample, and did not perform further star/galaxy discrimination for fainter objects.

For the objects with spectroscopic redshift, we also computed the photometric redshifts in order to test the accuracy of photometric redshift estimate for our filter set. Figure 2 shows the comparison between the spectroscopic redshifts and the photometric redshifts for those objects in our $H_{160} < 26$ catalogue. The spectroscopic and the photometric redshifts agree well within $\Delta z = 0.11$ over the wide redshift range except for the several outliers in the cases when the redshift probability function has a single dominant peak in the photometric-redshift measurement. We note, however, that there may be some systematic offset at $z \sim 1$; the photometric redshift is tend to be smaller than the spectroscopic ones. Further, in Figure 3, we compared the *hyperz* output with other photometric redshift by Fernandez-Soto et al. (1999). While our photometric redshift is calculated from HST $U_{300}, B_{450}, V_{606}, I_{814}, J_{110}, H_{160}$ -band data, the photometric redshift of Fernandez-Soto et al. (1999) is derived from HST $U_{300}, B_{450}, V_{606}, I_{814}$ -band data + KPNO J, H, K -band data (Dickinson 1998). Figure 3 shows the comparison between these two photometric redshifts of $H_{160} < 24.5$ galaxies which we can identified in common. Although over all correspondence is relatively good, there is the similar systematic offset at $z \sim 1$. There are also more than several outliers at $0 < z < 2$. We will study the possible influence of these features on our conclusion later in section 3.

For the sample selection in studying the evolution of the Hubble sequence along the redshift, we adopted the rest-frame V -band magnitude, M_V . The M_V values of the galaxies can be estimated from the observed data to $z = 2$ by interpolation and without extrapolation. Compared to the UV luminosity, rest-frame V -band luminosity is relatively insensitive to the on-going star formation activity for a given stellar mass and the extinction by dust. M_V (standard system) value of each object is calculated using the redshift adopted above (spectroscopic or photometric), assuming $H_0 = 70$ km/s/Mpc, $\Omega_0 = 0.3$, $\Omega_\Lambda = 0.7$.

From the $H_{160} < 26$ catalogue, 94 galaxies with $M_V < -20$ at $z < 2$ were selected as our final sample (50 with spectroscopic redshift, 44 with photometric redshift). In Figure 1, we also show the distribution of H_{160} -band magnitude of these $z < 2, M_V < -20$ galaxies. All the galaxies with

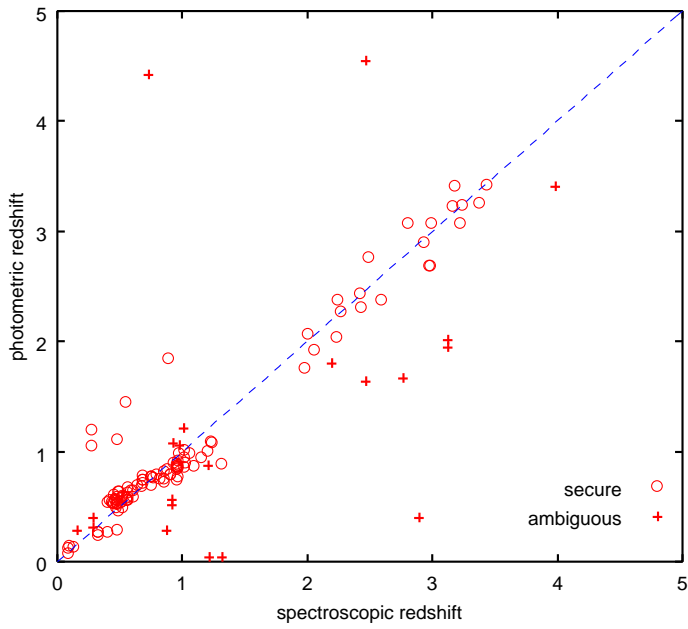


Fig. 2.. Comparison between the spectroscopic redshift and the photometric redshift of the $H_{160} < 26$ galaxies with spectroscopic redshift. Circles represent the galaxies whose redshift likelihood function of photometric redshift have single dominant peak, while crosses show those sources for which photometric redshift technique failed to constrain their redshift strongly.

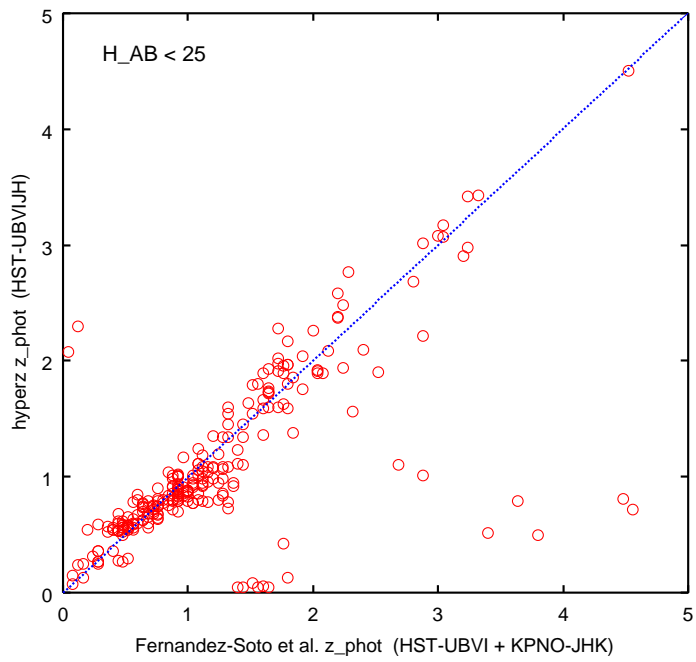


Fig. 3.. Comparison of different photometric redshifts of galaxies with $H_{160} < 24.5$. *hyperz* output with HST WFPC2/NICMOS U_{300} , B_{450} , V_{606} , I_{814} , J_{110} , H_{160} -bands vs Fernandez-Soto et al.'s catalogue with HST U_{300} , B_{450} , V_{606} , I_{814} -bands + KPNO J , H , K -bands.

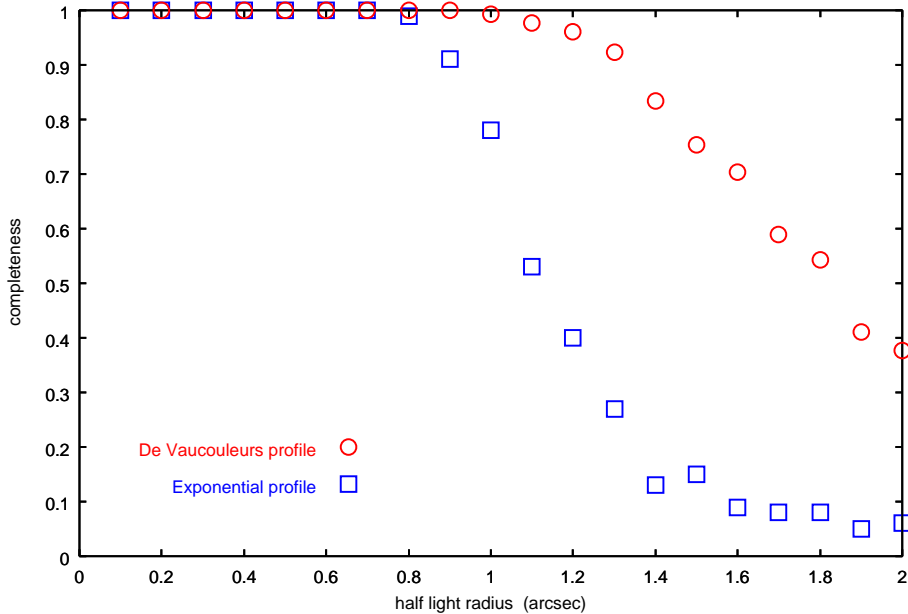


Fig. 4.. Detection completeness of $H_{160} = 24.5$ galaxies as a function of half right radius. Circles show that for de Vaucouleurs surface brightness profile, and squares represent that for exponential profile.

$M_V < -20$ at $z < 2$ are brighter than $H_{160} = 24.5$, which corresponds to $M_V \sim -20$ at $z = 2$ for our assumed cosmology, and thus at least 1-1.5 mag brighter than the turn around in the number counts at $H_{160} = 25.5$ -26 mag. In Figure 4, we investigate the detection completeness of $H_{160} = 24.5$ objects with various sizes by adding to the observed H_{160} -band frame the artificial galaxies with de Vaucouleurs or exponential surface brightness profile produced with *IRAF ARTDATA* package. All these artificial galaxies are face-on to measure the completeness conservatively. From the figure, our source detection seems to be complete to the half light radius of 0.8 arcsec for exponential profile, and 1.3 arcsec for de Vaucouleurs profile, which correspond to 6.5 kpc and 10.5 kpc at $z \sim 1$ -2 respectively for our adopted cosmology. Although some low surface brightness galaxies escape from our detection, the detection completeness of the galaxies in the Hubble sequence with the normal surface brightness must be very high above $H_{160} = 24.5$.

On the other hand, if the galaxy with $M_V < -20$ at lower redshift has $H_{160} > 24.5$, the galaxy must have unrealistically extremely blue SED between the observed band corresponding to rest- V band and the H_{160} -band, since the observed magnitude corresponding to rest-frame V -band becomes relatively bright. For example, we construct the constant SFR model spectrum of 1 Myr old with 1/50 solar metallicity whose SED can be approximated as $f_\nu \sim \nu^{1.25}$, using GISSEL code, and calculate the expected H_{160} -band magnitude of the $M_V = -20$ galaxy with such extremely blue SED for each redshift. The result is showed

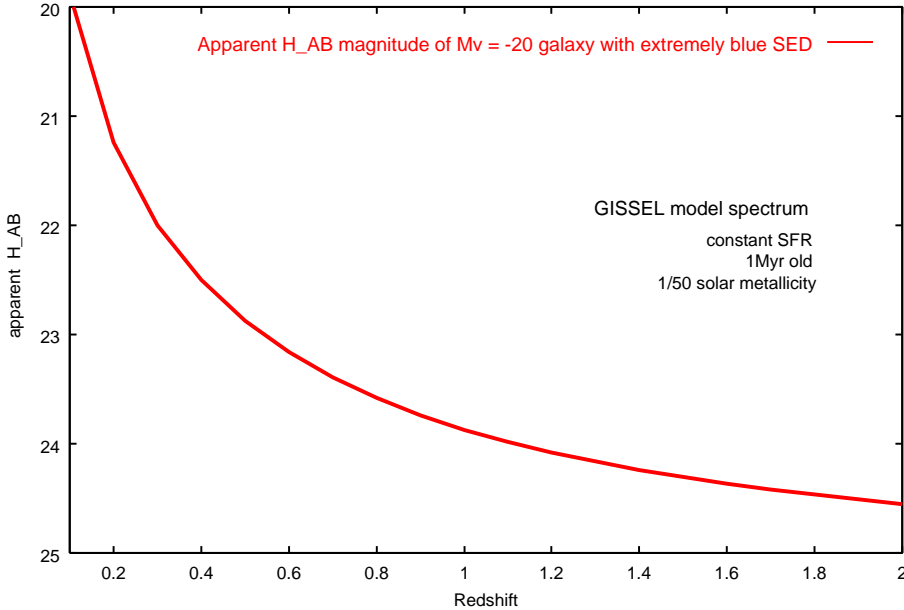


Fig. 5.. Predicted apparent H_{160} magnitude of $M_V = -20$ galaxies with very blue SED as a function of redshift. The model spectrum used for calculation is constant SFR model of GISSEL synthetic library with 1Myr age and 1/50 solar metallicity.

in Figure 5, and it seems that even the galaxy with such a blue spectrum has $H_{160} < 24.5$, if it satisfies $M_V < -20$.

Therefore, we believe that our $H_{160} < 26$ source detection can completely sample the $M_V < -20$ galaxies at $z < 2$ in very strict sense (for the adopted cosmological parameters).

2.4. Morphological Classification

We could visually classify the galaxy morphology but it is rather difficult to assign the morphological type to such faint objects and uncertainties can be large and unknown systematic error could exist. Instead, we performed the quantitative morphological classification for the $z < 2$, $M_V < -20$ galaxies using the I_{814} , J_{110} , H_{160} -band HST images so that the classification is made on the rest-frame V to I -band image for each object (I_{814} -band for $z < 0.5$, J_{814} -band for $0.5 < z < 1.0$, H_{160} -band for $1.0 < z < 2.0$), where the effects of K -correction or star-forming region on their morphology are relatively small. The classification method used is based on the central concentration index, C , and the asymmetry index, A (Abraham et al. 1996).

Our procedure for measuring the C and A indices followed Abraham et al.(1996), except that

we adopted the centering algorithm of Conselice et al.(2000). Early-type galaxies show strong central concentration in their surface brightness distribution, while late-type galaxies have a lower concentration. Those galaxies with a high asymmetry are classified as Irregular galaxies.

Since the C and A indices depend on object brightness, even if the intrinsic light profiles are identical, we evaluated the values by comparing the observed galaxy morphology with those of a set of simulated artificial ones that have similar photometric parameters as each observed galaxy in the following manner.

First, a large number (~ 50000) of artificial galaxies with pure de Vaucouleurs (bulge) or pure exponential (disk) profile with a wide range of half light radius and effective surface brightness are constructed using the *IRAF ARTDATA* package and added to the observed images. In addition to magnitudes and sizes (ISO_AREA from SExtractor), the C and A indices of these artificial galaxies were measured in an identical manner to the observed one. For each observed galaxy, the sample of the artificial galaxies with similar isophotal magnitude, isophotal area and axial ratio was constructed, and the C and A indices of the observed object were compared with the distribution of the indices of these artificial sample.

First, we examined the A values of the representative bright irregular galaxies, and adopted $A > 0.12$ as the criterion of “Irregular” category. In fact, of the objects with $A > 0.12$, those galaxies whose A index is greater than the median value of the artificial galaxy sample mentioned above at 2σ level are classified as “Irregular”. This criterion of 2σ above the sample of artificial galaxies with no intrinsic irregularity prevents relatively faint galaxies with intrinsically symmetric light profiles from being classified as irregular due to the effect of the background fluctuation.

For the galaxies which are not entered into the category of irregular galaxy, we then compare their C indices with those of the artificial sample. Each observed galaxy is classified as compact, bulge-dominated, intermediate, disk-dominated, irregular, respectively, according to its C value relative to the de Vaucouleurs profile sample and the exponential profile sample. For this purpose, the average value and the standard deviation of C index of the artificial galaxies are calculated for exponential sample and de Vaucouleurs sample, respectively with 3σ clipping (hereafter, these values refer as C_{dev} , σ_{dev} , C_{exp} , σ_{exp}).

Table 1 shows the conditions for each morphological category.

First, those galaxy whose C index ranges within 1σ of *both* de Vaucouleurs and exponential samples are classified as ‘cannot classify’. For those sources, the both sample of artificial galaxies have similar (low) C value due to their faintness, regardless of their surface brightness profile.

For the other observed galaxies, the C indices of the de Vaucouleurs and exponential profile samples show distinctive distributions. If there are some observed galaxies whose C value is significantly larger than those of de Vaucouleurs profiles, they are to be classified as ‘compact’, there is no such an object in our observed $z < 2$, $M_V < -20$ sample. On the other hand, we classify those galaxies that show

Fig. 6..

significantly lower or no concentration than that expected from exponential profile into the ‘irregular’ category. ‘Intermediate’ galaxies are those whose C value is intermediate between the distributions of de Vaucouleurs and exponential samples, which are separate each other. The galaxies whose C values correspond to those of de Vaucouleurs sample are classified as ‘bulge-dominated’, and those whose C values locate within the range of exponential sample are entered into ‘disk-dominated’ category.

In Figure 6, we show the montage of those galaxies classified into each category. The images in the figure are showed in pseudo-color produced from roughly rest-frame U , B , V -band ($U_{814}V_{606}I_{814}$ -band for $z < 0.5$, $B_{450}I_{814}J_{110}$ -band for $0.5 < z < 1.0$, $V_{606}J_{110}H_{160}$ -band for $1.0 < z < 2.0$). The each row corresponds to each redshift bin, and in each row, galaxies are aligned in order of the rest-frame $U - V$ color. As seen in Table 1, of 94 galaxies in $z < 2$, $M_V < -20$ sample, 19 galaxies are classified as bulge-dominated, 13 galaxies as intermediate, 32 galaxies as disk-dominated, 27 galaxies as irregular. The other 3 objects cannot be classified, and they are all located at $z > 1.5$.

Figure 7 shows an example of the morphological classification procedure mentioned above. In the figure, solid point shows the C value of an observed galaxy, while the histograms show the distributions of the de Vaucouleurs and exponential artificial samples for this object. The dotted lines represent the median C value (vertical) and the standard deviation (horizontal) of each artificial sample. The arrows under the figure shows each morphological region for this observed object derived from the conditions in Table 1, and this object is classified as disk-dominated.

For Cohen et al.(2000)’s sample, van den Bergh et al.(2000) performed visual classification, and their result can be used for testing the relation between our C/A classification and ordinal Hubble sequence scheme. This comparison is showed in Figure 8, where the morphological distribution of van den Bergh’s classification is showed for each morphological category by C/A classification in I_{814} -band according to van den Bergh et al.(2000). Shaded regions represent the galaxies with peculiarity in van den Bergh classification, such as “Sab pec”. The figure shows that our quantitative C/A classification correlates well with eyeball classification by van den Bergh, although some scatter exists. Most ‘bulge-dominated’ galaxies are classified as “E”, ‘disk-dominated’ galaxies corresponds to mainly spirals, and ‘irregular’ galaxies are “Irr” or galaxies with peculiarity in van den Bergh classification. Intermediate galaxies scatter around the early-type spiral.

We prefer to use quantitative morphological classification, because it is not only more objective but also can be taken into account of the effect of magnitude/surface brightness bias for classification by using the artificial galaxies with the same magnitude/surface brightness as observed objects as mentioned above.

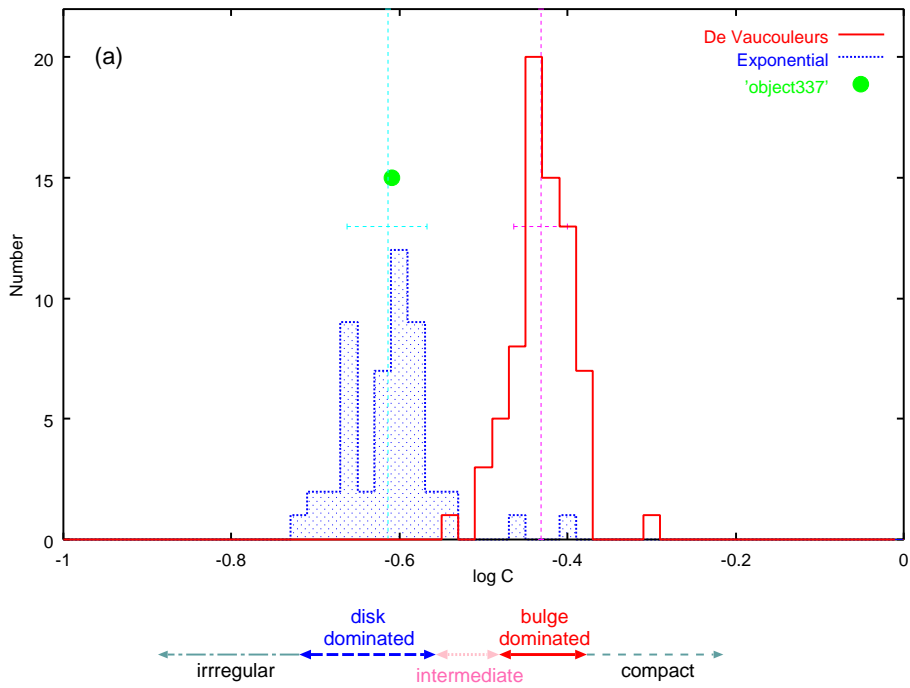


Fig. 7.. An example of morphological classification. This observed object has low A index value and is not irregular. Solid point shows the C index value of this object. Solid and dotted histograms represent the distribution of the C indices of the artificial De Vaucouleurs and exponential samples. Dashed lines shows the average value and the standard deviation of each artificial sample. Arrows under the figure represent the corresponding morphological region of C value derived from the condition in Table 1.

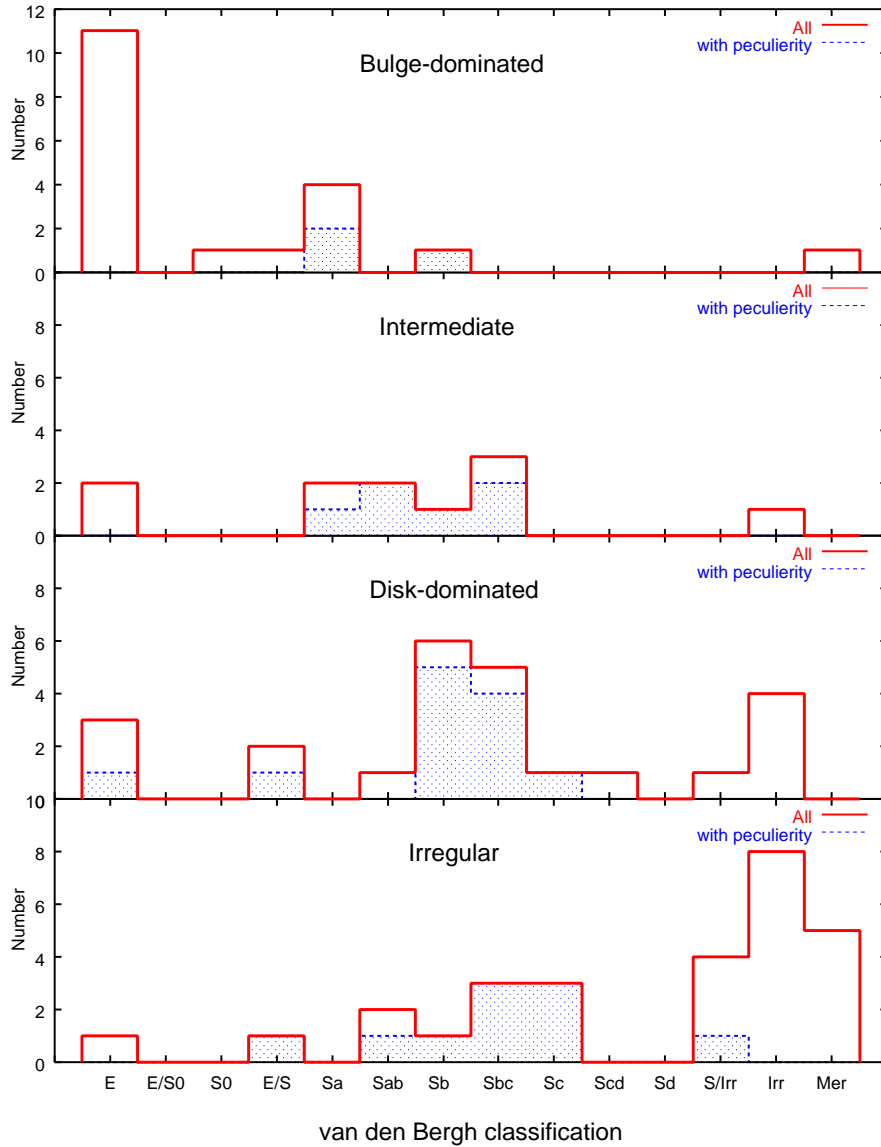


Fig. 8.. Comparison of morphological classification. Distribution of the visual classification from van den Bergh et al. (2000) is showed for the galaxies of each C/A classification morphological category. Shaded region represents the galaxies with peculiarity in van den Bergh classification.

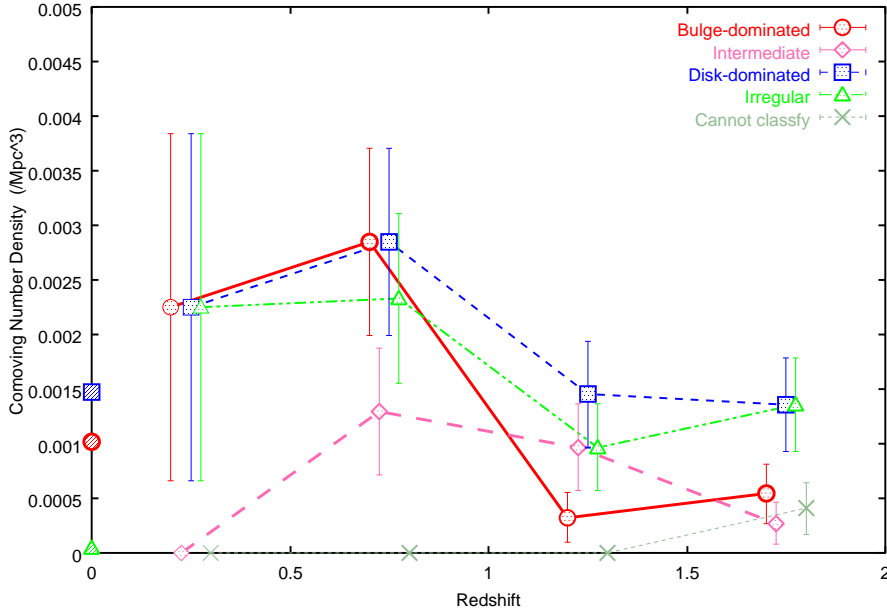


Fig. 9.. Evolution of morphological comoving number density of galaxies with $M_V < -20$. Each symbol represent morphological type. Circles: bulge-dominated, diamonds: intermediate, squares: disk-dominated, triangles: irregular, crosses: cannot be classified. Error bars are based on the square root of observed number. Hatched symbols at $z = 0$ show the number density of local galaxies calculated from the results of SSRS2 (Marzke et al. 1998): E/S0 (circles), Spiral (Squares), Irr/Pec (triangles).

3. Results

Using the volume-limited sample of $z < 2$, $M_V < -20$ galaxies mentioned above, we investigate the evolution of morphological comoving number density and their rest-frame color distributions to $z = 2$.

3.1. Morphological Comoving Number Density

Figure 9 shows the evolution of the morphological comoving number density of the $M_V < -20$ galaxies in the HDF-N. Each symbol represents the morphology classified in the previous section, and error bars are based on the square root of the observed number. We divided the redshift range $0 < z < 2$ into the four $\Delta z = 0.5$ bins, considering the number of the objects in each bin. The cosmology of $H_0 = 70$ km/s/Mpc, $\Omega_0 = 0.3$, $\Omega_\Lambda = 0.7$ is assumed.

For comparison, the local number density of each morphology (E/S0, Spiral, Irr/Pec) from Second Southern Sky Redshift Survey (Marzke et al. 1998) is plotted at $z = 0$, assuming the $B - V$ color of

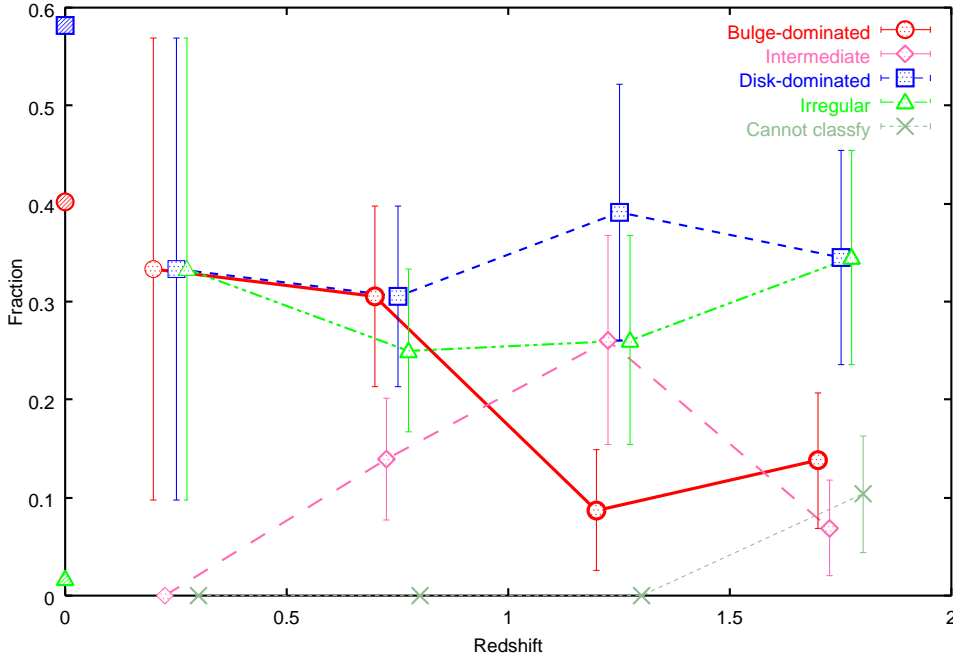


Fig. 10.. Evolution of morphological fraction of galaxies with $M_V < -20$. Each symbol is the same as in Figure 9.

empirical spectral templates for each morphology (Coleman et al. 1980).

In Figure 9, except for the lowest redshift bin where the sample is very small and statistical uncertainty is large, it is seen that the comoving density of $M_V < -20$ galaxies decreases at $z > 1$ in each morphological category. In particular, the number density of bulge-dominated galaxies conspicuously decreases to 1/5 between $0.5 < z < 1.0$ bin and $1.0 < z < 1.5$ bin.

In Figure 10, we show the evolution of the morphological *fraction* of $M_V < -20$ sample. As well as Figure 9, the local morphological fraction from SSRS2 is plotted at $z = 0$. Conspicuous features are that while at $0.5 < z < 1.0$, the fraction of irregular galaxies increases from local value, at $z > 1$, that of bulge-dominated galaxies decreases to about 1/3 of $0.5 < z < 1.0$ value. The fractions of irregular and disk-dominated galaxies slightly increase between $0.5 < z < 2.0$. This evolution of the relative abundance of each morphological class seems to reflect the differences of the luminosity or/and number evolution between morphological classes.

Before considering the origin of the decrease of number density of bright galaxies, we check our results for some points.

First, we investigated the behavior for the different set of the cosmological parameters. For the Einstein de Sitter model, $H_0 = 50$, $\Omega_0 = 1.0$, the trend seen in Figure 9 does not change significantly as

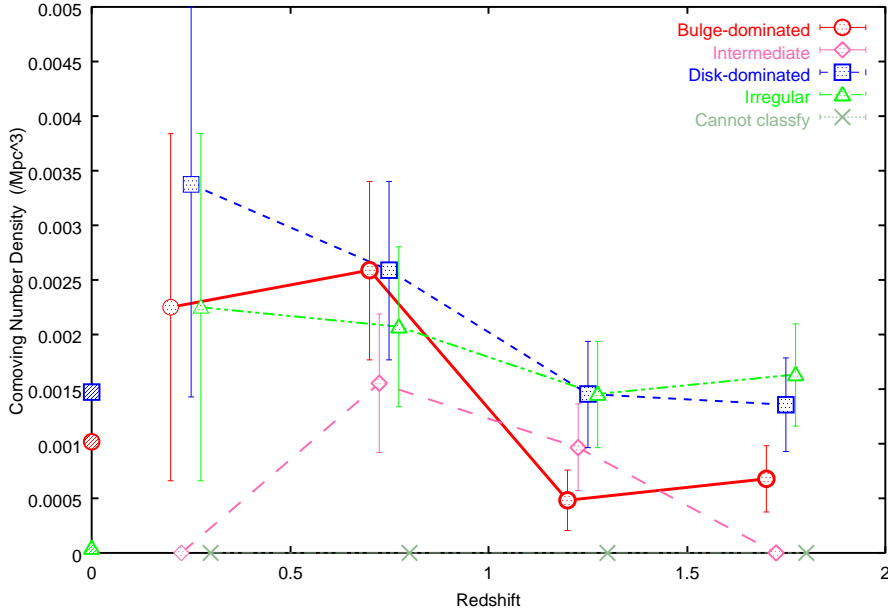


Fig. 11.. Same as Figure 9, but for the cosmology of $H_0 = 50$, $\Omega_0 = 1.0$.

shown in Figure 11.

Second, as mentioned in section 2.4, we performed morphological classification using different image for each redshift bin (I_{814} -band for $z < 0.5$, J_{110} -band for $0.5 < z < 1$, H_{160} -band for $1 < z < 2$), and this may cause systematic effects on the evolution of morphological number density. In order to check this point, we compared the classifications in the different bands.

Table 2 and 3 shows these comparisons, I_{814} -band classification vs. J_{110} -band one for $0.3 < z < 0.8$ galaxies, J_{110} -band vs. H_{160} -band for $0.7 < z < 1.3$ galaxies. Although there is some scatter, especially in Table 3 probably due to the relative faintness of sample galaxies, the agreements in these figures are relatively good and no strong systematic is seen. If we allow the exchange between bulge-dominated and intermediate or disk-dominated and intermediate, 16/20 in Table 2 and 31/37 in Table 3 agree with each other. Therefore, the transfer of the image used for classification at $z = 0.5$ and $z = 1$ does not seem to cause systematic effect on each redshift bin.

Third, as seen in Section 2.3, our photometric redshift seems to have systematic offset relative to spectroscopic redshift and other photometric redshift at $z \sim 1$, where the decrease of the comoving number density of the bright galaxies is seen. In order to investigate the effect of this feature, we repeated the same analysis as in Figure 9 using the Fernandez-Soto et al.'s photometric redshift. Of 166 $H_{160} < 24.5$ objects with no spectroscopic redshift, 151 objects can be found in Fernandez-Soto et al.'s catalogue. For the other 15 objects, the photometric redshifts by *hyperz* were used. Of these 15 objects, 13 objects have

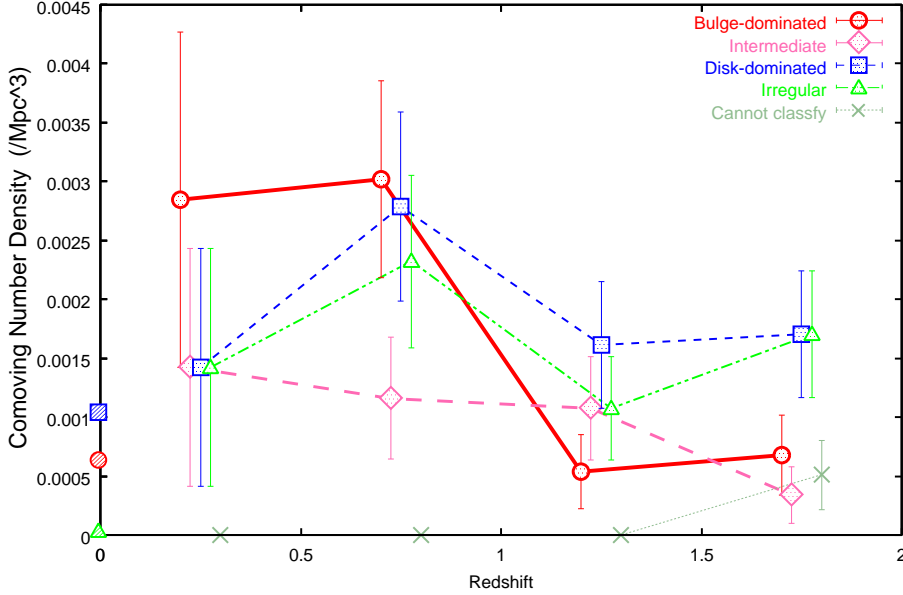


Fig. 12.. Same as Figure 9, but using the photometric redshifts from Fernandez-Soto et al(1999) for the galaxies without spectroscopic redshift.

$z_{phot} < 2$, and three of the 13 objects have $M_V < -20$. They are disk-dominated and irregular, and both located $1.5 < z_{phot} < 2.0$ range.

The result is shown in Figure 12. The decrease of the number density in each morphology become slightly more marginal. While the number density of disk and irregular galaxies may be constant at $0.5 < z < 2$, the decrease in bulge-dominated galaxies seems to remain significant in Figure 12.

The photometric redshift technique sometimes failed to constrain the redshift of the objects especially for the blue flat SED and for the smoothly red SED (produced by ‘blue flat SED + dust extinction’). In addition to the comparison between the different photometric redshifts with different filter set mentioned above, we estimate the effect of this intrinsic uncertainty of the photometric redshift by investigating the redshift likelihood function of each object outputted by *hyperz*.

The redshift likelihood functions of the 166 $H_{160} < 24.5$ galaxies with no spectroscopic redshift were investigated, and the secondary peak whose amplitude is greater than a fifth of the primary peak (i.e., best-fit z_{phot}) were checked. Of 166 sources, 38 objects have these secondary peaks. For each redshift bin in Figure 9 (and for each morphology), we counted possible number of the objects which are escaped from or entered into each redshift bin if their secondary peaks represent the true redshift. The number of galaxies in each redshift bin and these possible escaped and included number for the secondary peak redshift are shown in Table 4.

The effect of this uncertainty is negligible at $z < 1$ due to the dominance of spectroscopic sample in this redshift range. It is seen that at the uncertainty of the disk-dominated and irregular galaxies is relatively large at $z > 1.5$, while the bulge-dominated or intermediate galaxies is scarcely affected.

In summary, we found that while the rapid decrease of the number density of the bulge-dominated galaxies with $M_V < -20$ at $z > 1$ may not be much affected by the uncertainty of the photometric redshift, the decrease of the number-density of the disk-dominated or irregular galaxies are rather marginal and to be widely tested and to be confirmed with the large sample in the future. It is also very desirable to obtain the firm spectroscopic redshifts for the objects at $1 < z < 2$.

3.2. Rest-frame $U - V$ Colors

Galaxies in the Hubble sequence in the local universe also lie on the sequence in the $U - V$ and $B - V$ two color diagram (Huchra 1977; Kennicutt 1983). In other words, galaxy SED can be characterized by the rest-frame $U - V$ color because the color is sensitive to the existence/absence of the largest features in galaxy continuum spectra at near-UV to optical wavelength, namely, 4000 Å break or the Balmer discontinuity. If the stellar population in the galaxies changes along the redshift, the Hubble 'color' sequence seen in the local universe must also change at high redshift. In this subsection, we trace the color evolution of the galaxies with $M_V < -20$ at $z < 2$.

By using WFPC2 U_{300} , B_{450} , V_{606} , I_{814} and NICMOS J_{110} , H_{160} -band data, we can measure the rest-frame color blue ward rest-frame V -band of the $z < 2$, $M_V < -20$ galaxies without extrapolation. The rest $U - V$ color of each object is calculated from the best-fit SED template in the photometric redshift technique and the standard Johnson U and V -band filter through put (for those with spectroscopic redshift, the similar SED fit with broad band data was performed, fixing the redshift). Figure 13 shows the evolution of the rest $U - V$ color distribution (standard Johnson-like system) with M_V value of the $M_V < -20$ galaxies for each morphology. For comparison, at the top of each figure, the typical $U - V$ color of local galaxies is indicated for each morphology (Bershady et al. 2000).

In Figure 13a, the color distribution of bulge-dominated galaxies (shaded circle) is showed with intermediate galaxies (open circle). The bulge-dominated galaxies show the relatively broad color distribution, from the similar red color with local early-type galaxies to blue color of local Sc galaxies ($U - V \sim 0.5$) at $z < 1$. At $z > 1$, although the number of the galaxies in each bin is rather small, some blue ($U - V < 0.3$) bulge-dominated galaxies are seen, while there are also the galaxies with red rest $U - V$ color which is consistent with passive evolution model ($U - V \sim 1$) with large formation redshift. For the intermediate-type galaxies, the similar trend is seen.

Figure 13b shows the similar diagram for disk-dominated galaxies (shaded circle) with intermediate ones (open circle), as Figure 13a. The rest $U - V$ color distribution of disk-dominated galaxies at $z < 1.5$ cover the wide range which corresponds to local Sa-Irr color ($U - V \sim 0.1-1.2$). There are also a few bluer galaxies with $U - V < 0.1$, and their fraction seems to increase with redshift.

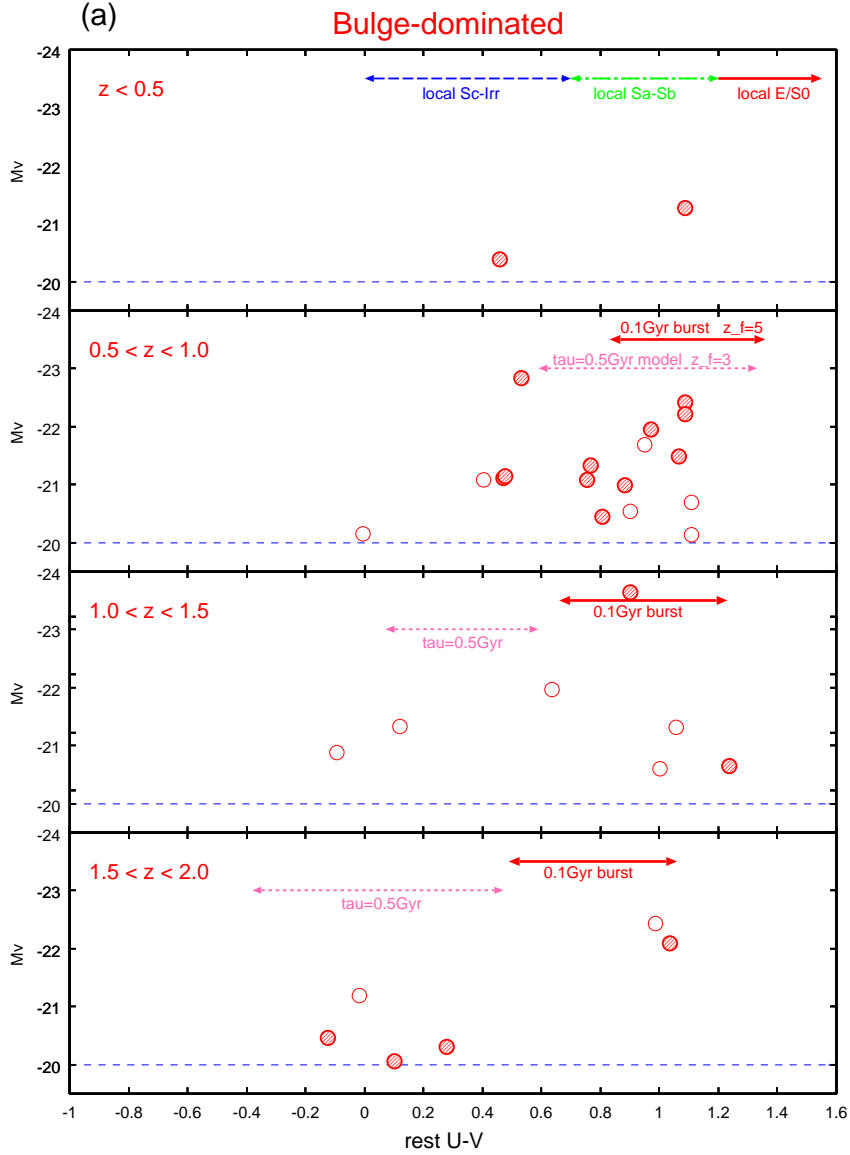


Fig. 13.. Rest-frame $U - V$ color distribution of $M_V < -20$ galaxies in each morphology. Each row corresponds to each redshift bin. Vertical axis in each row represents the rest-frame V absolute magnitude. Arrows in the top row represent the corresponding range of rest-frame $U - V$ color of typical local galaxies with each morphological type.

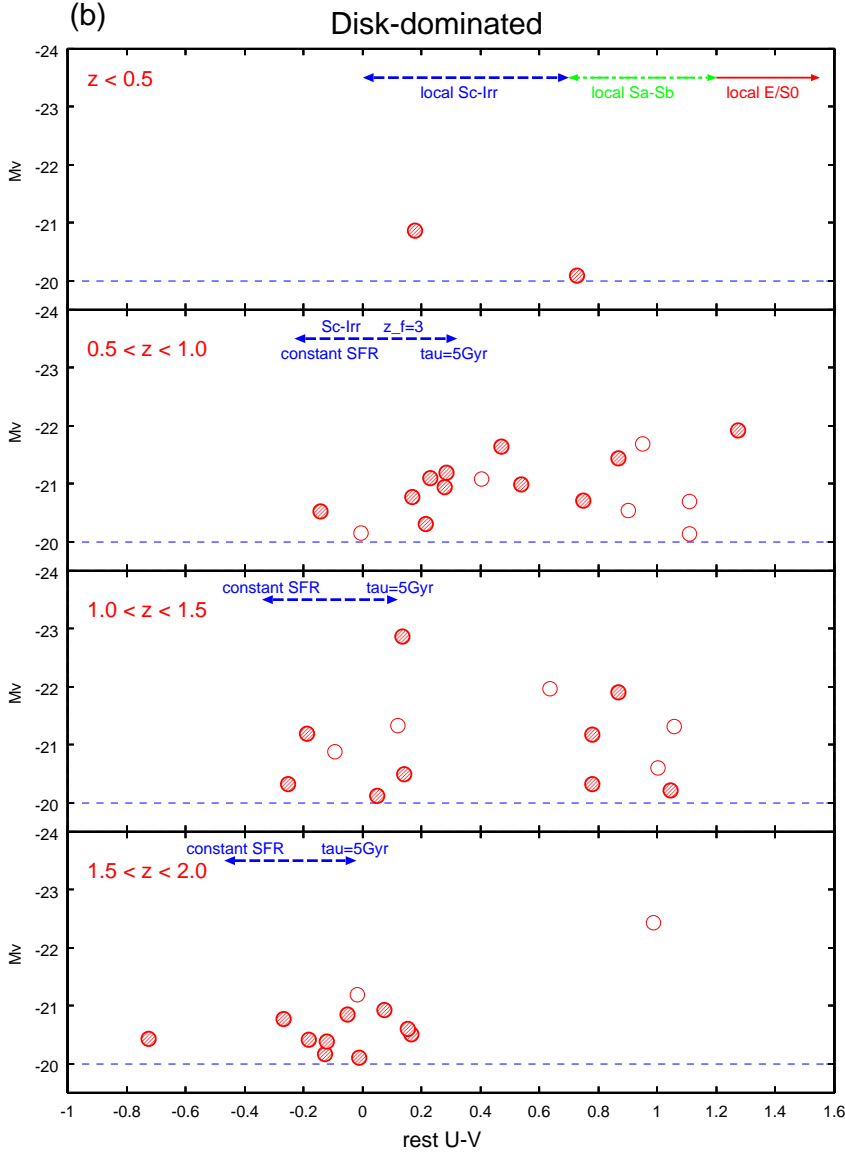


Figure 13 continued

At $z > 1.5$, all the disk-dominated galaxies in our sample have $U - V < 0.3$. Since about 40% of the disk-dominated galaxies have $U - V > 0.3$ at $z < 1.5$, the significant change of the rest $U - V$ color distribution seems to occur at $z \sim 1.5$.

In Figure 13c, most irregular galaxies show the relatively blue color of $U - V \sim 0$, which is similar to or slightly bluer than local Irr galaxies, while there are also a few red irregular galaxies. At $z > 1.5$, very blue galaxies with $U - V < -0.2$ occupy significant fraction of irregular, and there is no irregular

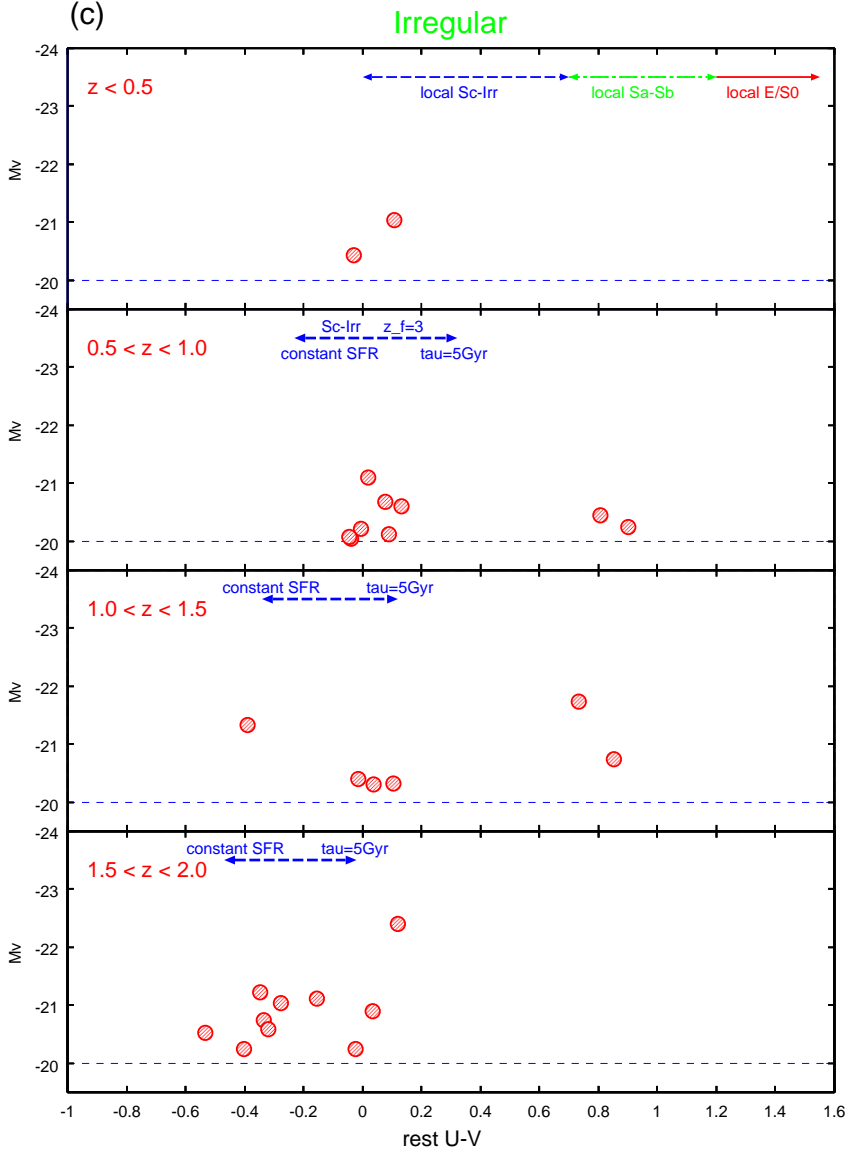


Figure 13 continued

galaxies with $U - V > 0.3$ as well as disk-dominated galaxies.

In Figure 14, in order to estimate the uncertainty of the rest-frame $U - V$ color due to the interpolation procedure, we compare the rest-frame $U - V$ color derived from SED fitting mentioned above with that calculated from linear interpolation between the nearest observed band data in f_λ . Although there is some uncertainty due to the interpolation, $\Delta U - V$ is at most 0.2 mag (mean and standard deviation values are 0.06 ± 0.13), and the trends seen in Figure 13 are not changed even if the

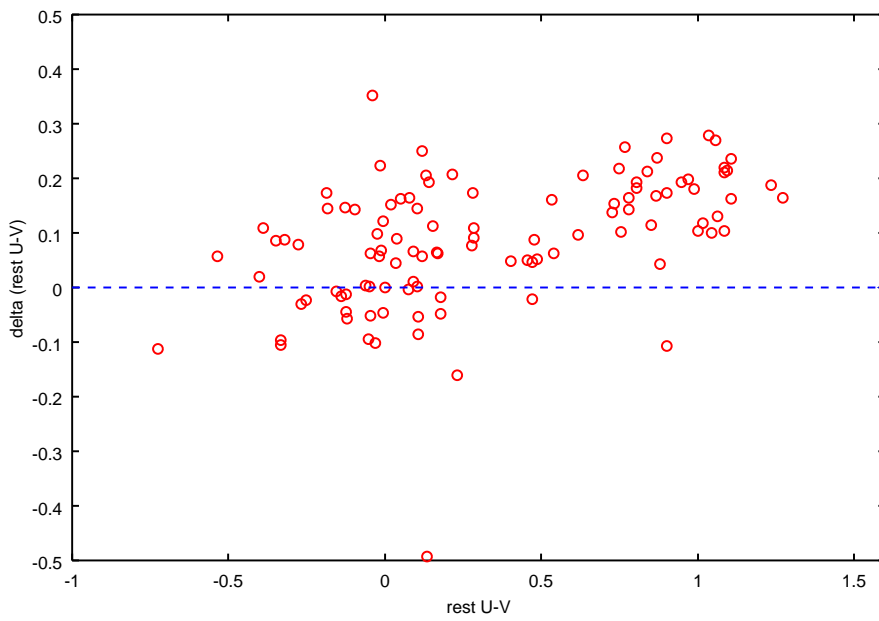


Fig. 14.. Differences between rest-frame $U - V$ colors derived from SED fitting with six HST bands and the linear interpolation from the nearest observed bands to rest U and V -band, as a function of $U - V$ value (of SED fitting).

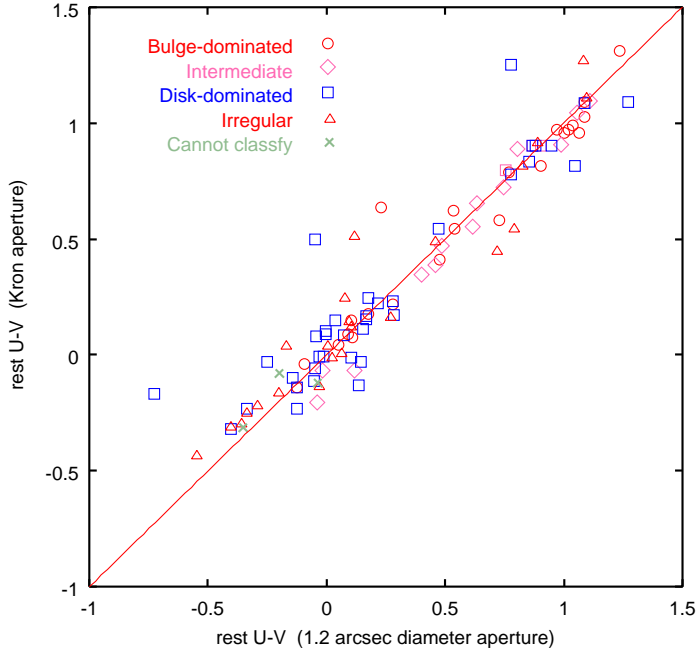


Fig. 15.. Comparison of rest-frame $U - V$ colors of $M_V < -20$, $z < 2$ galaxies measured with different aperture sizes: 1.2" diameter aperture vs Kron aperture. Each symbol represents morphological type.

colors derived from the linear interpolation of the nearest observed band data are used.

Further, in order to evaluate the aperture effect, we repeated the photometry with Kron aperture of H_{160} -band image of each objects, and compared rest-frame $U - V$ color calculated from this result with those from the 1.2 arcsec diameter aperture photometry (Section 2.2) in Figure 15. It is seen that the aperture effect does not affect strongly the results in Figure 13.

4. Discussion

4.1. Bulge-dominated Galaxies

In Figure 9, the number density of the bulge-dominated galaxies decreases rapidly at $z > 1$. In fact, the number density at $z > 1$ (two higher redshift bins) is about two times smaller than the local number density of early-type galaxies from the SSRS2 ($H_0 = 70 \text{ km s}^{-1} \text{ Mpc}^{-1}$, $\Omega_0 = 0.3$, $\Omega_\Lambda = 0.7$), although the significance is two sigma level due to the small statistics. When compared with the $0.5 < z < 1$ bin, the decrease become factor of five, which corresponds to $\gtrsim 3$ sigma significance.

4.1.1. Comparison with the Previous Studies at $z < 1$

First, before considering the possible physical explanation of the result, we compare our results of the earlier works although the galaxies treated in the previous studies are brighter than those studied in this paper at $z \gtrsim 0.8$.

To $z = 1$, Schade et al.(1999) investigated the evolution of the early-type galaxies with $I_{AB} < 22$ in the CFRS/LDSS surveys selected by 2D-fitting morphological classification with HST images, and found that the evolution of space density of those galaxies is consistent with pure luminosity evolution (no number density evolution) of $\Delta M_B \sim 1$ mag to $z = 1$, which was also observed in their size-luminosity relation and consistent with passive evolution model. The number density of $0.5 < z < 1$ bin in Figure 9 is 2.5 times larger than the local density of early-type galaxies in SSRS2 survey in the same absolute magnitude range, but considering the same luminosity evolution of $\Delta M_B \sim 1$ to $z = 1$, it is also consistent with pure luminosity evolution. In Figure 16a, we compare the evolution of the number density of bulge-dominated galaxies with the pure luminosity evolution model based on the local density of SSRS2 and the luminosity evolution of passive (single 0.1Gyr burst) model spectrum calculated by GISSEL code. Although there may be some marginal excess, the number density of $0.5 < z < 1$ bin is consistent with the passive evolution model with high formation redshift. For $H_0 = 50$, $\Omega_0 = 1.0$ cosmology (Figure 16b), the passive evolution model seems to underpredict the number density of early-type galaxies at $0.5 < z < 1$ (2.5σ level).

Schade et al.(1999) also claimed that the significant fraction ($\sim 30\%$) of their sample of early-type galaxies shows the rather bluer rest-frame $U - V$ colors than those expected from passive evolution model, and large [OII] equivalent width. Although their selection of $I < 22$ is about one magnitude brighter than our $M_V < -20$ selection at $z \gtrsim 0.75$, in Figure 13a, our bulge-dominated sample also shows the wide distribution of rest $U - V$ color, and some are ~ 1 mag bluer than those expected from passive evolution model, which is similar to Schade et al.

Menanteau et al.(1999) investigated the optical-NIR color distribution of the field early-type galaxies with $HK' \lesssim 20$, which are selected by quantitative classification with C and A indices in the HST images. They also found that at $z < 1$, the number density of luminous early-type galaxies is consistent with that expected from the local luminosity function, but their optical-NIR color is skewed blue-ward relative to the passive evolution model prediction. Their results agree with those of Schade et al. in that bright early-type galaxies is consistent with no number density evolution, but there are galaxies with bluer color than that expected from passive evolution model.

At $z < 1$, for low density totally flat universe, the result about the evolution of the bulge-dominated galaxies in our sample seems to be consistent with those of other studies, although our HDF-N data samples the fainter galaxies.

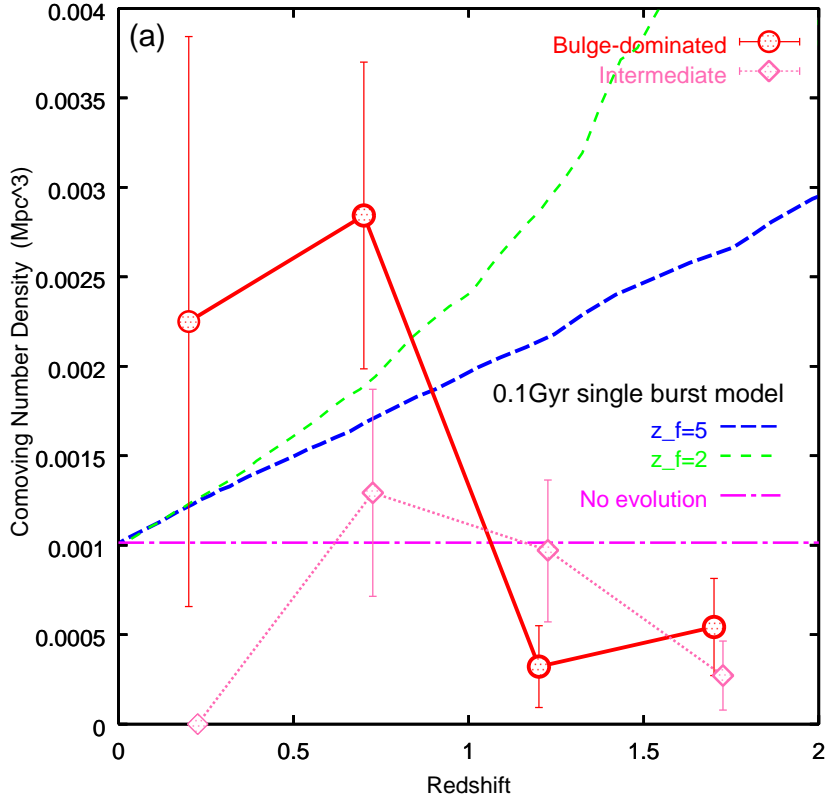


Fig. 16.. Comparison of the comoving number density evolution of bulge-dominated galaxies with pure luminosity passive evolution model. Circles represents number density of bulge-dominated galaxies, pentagon shows intermediate galaxies, which are same as in Figure 9. Model predictions (dashed and dotted curves) are calculated from local luminosity function of early-type galaxies from SSRS2 (Marzke et al. 1998) and the luminosity evolution derived from 0.1 Gyr single burst models of GISSEL library with formation redshift of two and five. a) for $H_0 = 70 \text{ km s}^{-1} \text{ Mpc}^{-1}$, $\Omega_0 = 0.3$ $\Omega_\Lambda = 0.7$ cosmology, b) for $H_0 = 50$, $\Omega_0 = 1.0$.

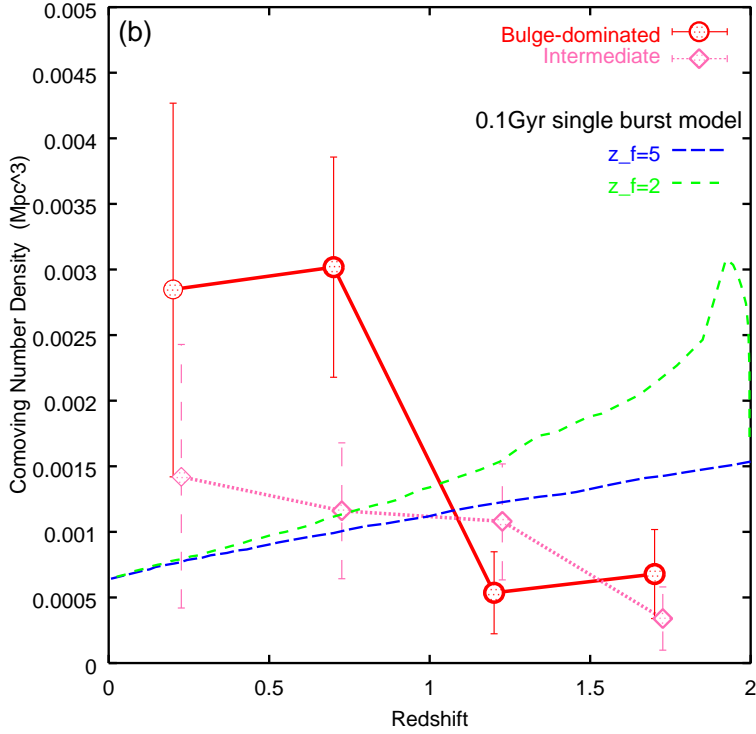


Figure 16 continued

4.1.2. Comparison with the Previous Studies at $z > 1$

On the other hand, while the passive evolution model predicts that the galaxies become more luminous as we approach the formation redshift, and the comoving number density of the fixed absolute magnitude limited sample increase with redshift, those of bulge-dominated galaxies decrease at $z > 1$. In Figure 16a, the deficit of bulge-dominated galaxies at $z > 1$ relative to the model prediction calculated from local number density and passive luminosity evolution is significant.

Several other studies investigated the number density evolution of early-type galaxies at $z > 1$ in the HDF-N. Franceschini et al.(1998) studied the ground-based K -selected ($K < 20.15$) early-type galaxies selected by light profile fitting morphological classification with WFPC2 image, and found that their redshift distribution is suddenly decrease at $z \sim 1.3$, which is consistent with our result. Rodighiero et al.(2001) recently added the same $K < 20.15$ sample in the HDF South WFPC2 and NICMOS fields to Franceschini et al.' sample, and confirmed the similar results. Franceschini et al.(1998) claimed that this decrease of early-type galaxies is caused by the morphological disturbance due to merging events and the dust obscuration in the starburst phase of these galaxies.

Note that their selection of $K < 20.15$ is about 1 mag brighter at $z \sim 1$, 2 mag at $z \sim 2$ than our

$M_V < -20$ selection. We thus confirm that the decrease of number density of these galaxies at $z > 1$ also seen for the less luminous galaxies down to the absolute magnitude corresponding to $\sim L_* + 1$.

Zepf (1997) found that there is no extremely red ($V_{606} - K > 7$) galaxies in the HDF-N, and concluded that no passively evolving galaxy at $z > 1$ with formation redshift $z_f \sim 5$ exists, and most early-type galaxies must have significant star formation at $z < 5$. In our volume-limited $M_V < -20$ sample, there are a few galaxies at $z > 1$ whose color is consistent with or slightly bluer than the passive evolution model with $z_f \sim 5$ in Zepf (1997) (corresponding rest $U - V \gtrsim 1-1.2$). Since the V_{606} -band traces rest-frame $< 3000\text{\AA}$ at $z > 1$, if only small star formation activities are occurred in these galaxies, the $V_{606} - K$ color can become bluer easily.

Dickinson (2000b) compared the comoving number density of the $M_V < -19$ galaxies in the HDF-N between $0 < z < 1.37$ and $1.37 < z < 2$, using the same WFPC2/NICMOS images as those used in this paper, and found the deficit of not only the early-type galaxies but of all the bright galaxies at high redshift, which is consistent with our result of Figure 9, although deficit of disk-dominated and irregular galaxies is rather marginal if the uncertainty of photometric redshift is considered in our analysis. He also pointed out that there are a few early-type galaxies with $z_{phot} \sim 1.8$ whose relatively red rest $B - V$ color is consistent with passive evolution model with $z_f \sim 4$ (in our sample, these galaxies correspond to bulge-dominated or intermediate galaxies with rest $U - V \sim 1.0$ in $z > 1.5$ redshift bin), and that bluer early-type galaxies are also found, which is seen in our Figure 13a, too.

4.1.3. Morphological Number counts in NIR

In order to avoid the uncertainty of the photometric redshift, we also compare the type-dependent number counts of the galaxies in the NICMOS H_{160} -band image with the model prediction. Figure 17 shows the H_{160} -band number counts of the bulge-dominated and intermediate galaxies. The model prediction from local luminosity function of early-type galaxies (Marzke et al. 1998) and passive evolution (0.1 Gyr single burst with $z_f = 5$) are also plotted. The upper curve represents the all early-type galaxies, and the middle and lower curves correspond to the contributions of those at $z < 2$ and $z < 1$, respectively. At $H_{160} > 21.5$, where the contribution of $z > 1$ galaxies increase in the passive evolution model, the observed number of bulge-dominated galaxies is clearly deficient, although if *all* intermediate galaxies are added, the observed number counts can explain the contribution of $z < 2$ early-type galaxies. This result seems to suggest that the decrease of bulge-dominated galaxies at $z > 1$ discussed above is not artifact due to the uncertainty of the photometric redshift technique.

4.1.4. Implication

In summary, in the HDF-N, the number density of bright ($\gtrsim L_V^* + 1$) early-type galaxies decreases at $z > 1$, being contrary to the prediction of passive evolution model with constant comoving number density. Further, their wide color distribution indicates the possibility that the mean stellar age of each

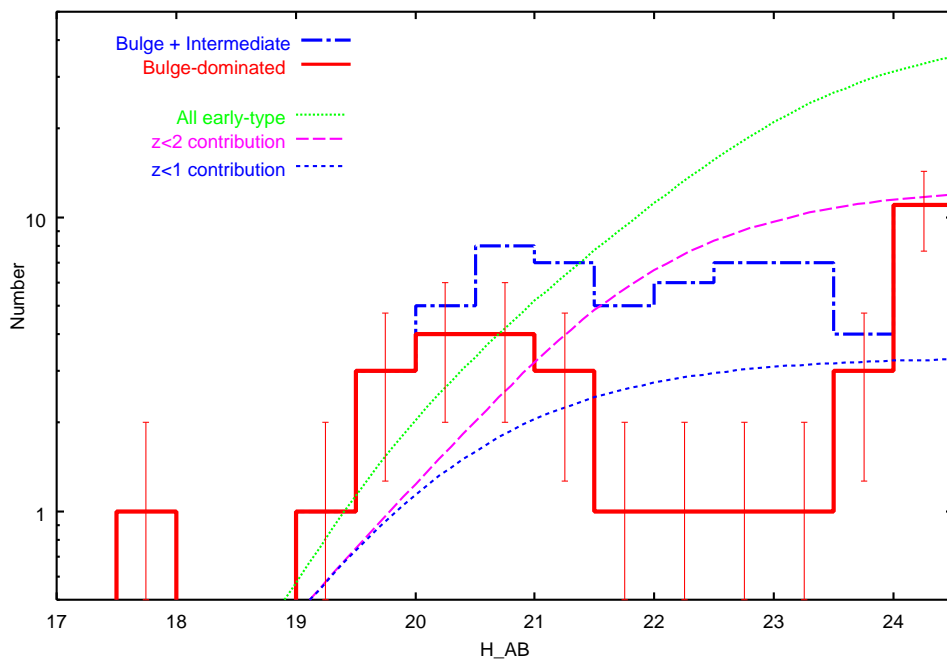


Fig. 17.. H_{160} -band number counts of bulge-dominated and intermediate galaxies. Solid histogram shows bulge-dominated only, and dotted-dashed histogram represents bulge-dominated + intermediate galaxies. The curves show the prediction of the pure luminosity passive evolution model (see text).

field early-type galaxy differs each other. It seems that significant fraction of early-type galaxies do not obey the passive evolution with high formation redshift, while there are some galaxies whose color is consistent with those models.

What causes the deficit of the red bulge-dominated galaxies in the HDF-N at $z > 1$ and how can we explain the blue colors of those *observed* at $z > 0.5$?

The decrease of number density of these galaxies at $z > 1$ seen in Figure 9 indicates that significant fraction of these $\gtrsim L_*$ early-type galaxies does not seem to have the appearance of the representative bright early-type galaxy at this redshift range. Since the similarly bright irregular galaxies do not show the corresponding rapid increase of the number density at $z > 1$ in Figure 9, and also not at the fainter galaxies in our $H_{160} < 26$ catalogue (e.g., $M_V < -19$ as we have confirmed although not shown in this paper in detail), the morphological disturbance due to the simple merging scheme seems to be difficult to explain the observed decrease of early-type galaxies.

As discussed in Franceschini et al.(1998), the dust obscuration may be important at these epochs. However, if the deficit of the galaxies with $M_V = -22$ at $z \sim 1.5$ is due to the dust extinction with $A_V \sim 1$ mag for example, we may expect as many early-type galaxies with *red* colors due to the dust extinction. In our HDF-N sample, the observed number density for the galaxies $M_V < -20$ is still very small and they tend to have *blue* $U - V$ color. There may be some misclassification in our sample but not that the colors of the galaxies in the rest of the sample with $M_V < -20$ (disk and irregular) are even bluer than those of the early-type objects. Therefore, only the dust model does not seem to be compatible with the observed results.

One possible explanation is that simply the formation (from the cold gas or gas-rich small progenitors) epoch of the early-type galaxies is at $z \sim 1.5-2$ and they are formed in with relatively short time scale and with highly spatially biased manner at higher redshift as expected for the CDM universe.

The galaxies formed at $z > 2$ may have red rest-frame $U - V$ color, but the chance to observe such object may be low if they are strongly spatially biased. Note that Steidel et al. (1998) and Adelberger et al. (1998) found the large clustering is seen for the Lyman-Break galaxies at $z \sim 3$. At ~ 10 Mpc scale, the 1-sigma fluctuation of the galaxy density is 3 to 6 times the mass fluctuation in the totally flat and the Einstein-de Sitter universe, respectively. Daddi et al. (2000) also found the very strong clustering for the galaxies with $K \sim 19$ and $R - K > 5$ that are consistent with the passively-evolving galaxies formed at $z > 3$.

If some galaxies are formed at rather low redshift, they may correspond to the density peaks with lower peak height and the clustering is less strong than those formed at higher redshift from higher density peak. They may appear in the absolute magnitude-limited sample but with relatively blue colors.

Indeed, several bluer bulge-dominated galaxies whose rest $U - V$ colors are similar to those of the local Scd galaxies (rest $U - V \sim 0.6$) exist in our sample, and at $z > 1$, there are still bluer bulge-dominated galaxies. We compared their color with single 0.1Gyr burst model of GISSEL code. In Figure

13a we show the prediction of the color range calculated from local color range with such passive evolution model with formation redshift of $z_f = 5$. Solar metallicity and Salpeter initial mass function are adopted. It is seen that the color of $U - V \lesssim 0.6$ is clearly bluer than the passive model with $z_f = 5$. Although still lower metallicity may be considered, it is difficult that this color of these bluer bulge-dominated galaxies is explained only by metallicity variation since the local populations of early-type galaxies have solar or sub-solar metallicity. It is plausible that these blue galaxies have some amount of star formation activity or the younger mean stellar age than passive evolving galaxies. In fact, at $z < 1$, Schade et al (1999) detected strong [OII] emission in the blue early-type galaxies. In Figure 13a, we also plot the exponentially decaying SFR model with $\tau = 0.5\text{Gyr}$, and such model with same formation redshift can roughly explain the observed data. Even in the cluster environments, a large fraction of the NIR-selected galaxies show the bluer colors than that expected from passive evolution models, and the blue color seems to be due to some amount of the star-formation activity (Tanaka et al. 2000; Kajisawa et al. 2000; Haines et al. 2001; Nakata et al. 2001).

The blue bulge-dominated galaxies at $z > 1$ tends to be relatively faint ($M_V \sim -20$) compared with $z < 1$ bulge-dominated galaxies, although their number is very small. If these blue galaxies halt star formation and evolve passively soon after the observed epoch, these will become fainter and these are not correspond to the ancestor of the $z < 1$ bulge-dominated galaxies with $M_V < -20$. If this is the case, the decrease of the number density of bright bulge-dominated galaxies at $z > 1$ can be more significant.

It should be noted that for $H_0 = 50$, $\Omega_0 = 1.0$ cosmology, the deficit of bulge-dominated galaxies relative to passive evolution model becomes to be rather marginal (Figure 16b). If all intermediate galaxies are added, the observed number density is consistent with the model prediction. In this case, as mentioned in Section 4.1.1, the observed number density significantly exceeds the model prediction at intermediate redshift. This may be explained as the cosmic variance due to the over density peak in redshift distribution discussed in Cohen et al.(2000).

4.2. *Disk-dominated Galaxies*

For disk-dominated galaxies, it is found that the rest-frame $U - V$ color distribution significantly changes from $z \sim 0.5$ toward $z \sim 2$ and there are some very blue galaxies with $U - V < -0.3$ while the comoving number density does not show significant evolution between $0 < z < 2$. At $z > 1.5$, the colors of the galaxies are found to be very blue ($U - V < 0.3$), and few objects have the $U - V$ colors such as seen for the local normal late-type galaxies. It is very likely that we see the galaxies at very young stage at $z > 1.5$.

4.2.1. *Comparison with the Previous Studies at $z < 1$*

At $z < 1$, our data suggest mild color and luminosity evolution for the population, which is consistent with the previous results obtained by various authors.

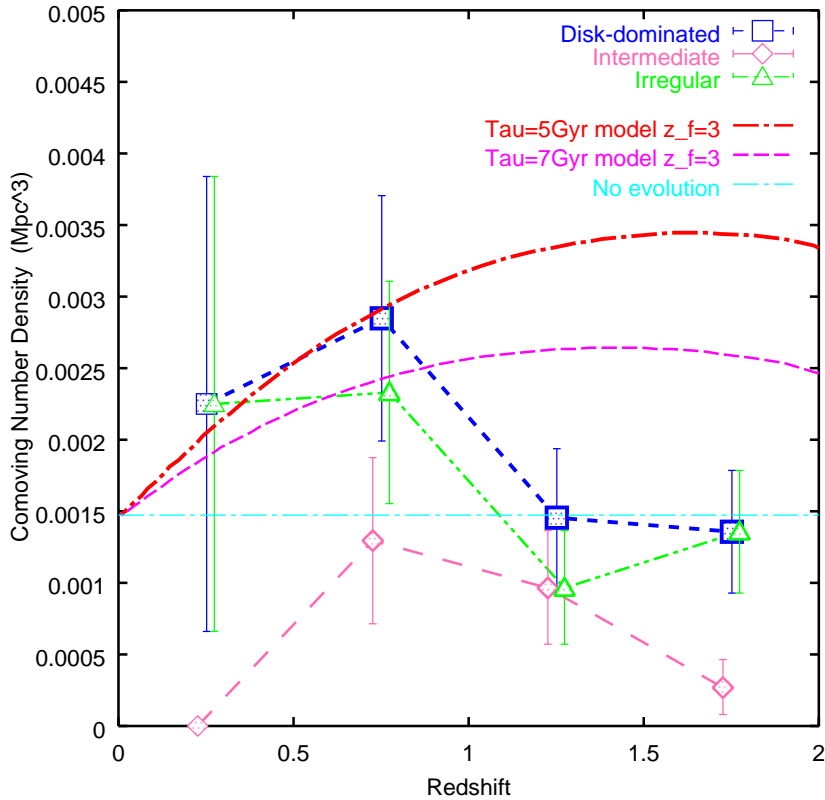


Fig. 18.. The similar figure with Figure 16 for disk-dominated galaxies. Squares represent the comoving number density of disk-dominated galaxies, pentagons represent that of intermediate galaxies, and triangles show irregular galaxies. The curves show prediction of the pure luminosity evolution models derived from local luminosity function of spiral galaxies (from SSRS2) and the exponentially decaying SFR model with $\tau = 7$ and 5Gyr.

Lilly et al.(1998) studied the disk-dominated galaxies selected by 2D-fitting classification in the CFRS/LDSS survey, and found that the size function of the relatively large (and bright) galaxies does not change at $0 < z < 1$ while the rest-frame B -band luminosity at $z \sim 0.7$ is ~ 0.5 mag brighter than the local value on the average. In Figure 18, we compare the comoving density of disk-dominated galaxies with such mild luminosity evolution (exponential decaying SFR model with $\tau = 7$ or 5Gyr) with constant number density. At $z < 1$, the observed number density is consistent with those model, as well as Lilly et al.

Vogt et al.(1996, 1997) confirmed that relatively bright ($\lesssim M_* + 1$) $z > 0.5$ disk galaxies have the rotation curve similar to that of local disk galaxies, and found that the similar rest B -band luminosity offset to local sample of ~ 0.5 mag in the Tully-Fisher relation and the surface brightness evolution.

These results seem to indicate that the bright disk galaxies in the present universe have already formed at $z \sim 1$.

In Figure 13b, we show the rest-frame $U - V$ color of the disk-dominated galaxies in the HDF-N. Lilly et al.(1998) pointed out that the average rest $U - V$ color of the $z > 0.5$ disk-dominated galaxies is slightly bluer (0.2-0.3 mag in their Figure 15) than local one. The average color of the disk-dominated galaxies in the $0.5 < z < 1$ bin in our sample is $U - V \sim 0.25$, which is slightly bluer than that obtained by Lilly et al.(1998). If we consider, however, the uncertainty due to the interpolation and the aperture effects in evaluating the rest $U - V$ color (Figure 14 and 15), the averages of the both samples is in fact consistent with each other.

Lilly et al.(1998) interpreted the mild color evolution as the modest increase of star formation in the bright disk-dominated galaxies at $z > 0.5$, and pure luminosity evolution model with the exponentially decaying star formation rate with $\tau = 5\text{Gyr}$ and $z_f = 4$ can roughly explain these observed trend.

4.2.2. Evolution of Disk-dominated Galaxies at $z > 1$

At $z > 1$, while the rest $U - V$ color distribution of the disk-dominated galaxies in the $1 < z < 1.5$ bin is wide-spread, which is consistent with mild evolution seen at $0.5 < z < 1$, *all* disk-dominated galaxies in the $1.5 < z < 2.0$ bin have rest $U - V < 0.3$, which is clearly bluer than local late-type spirals. In Figure 13b, we plot the model prediction of rest $U - V$ distribution based on local value, whose upper limit is determined by $\tau = 5\text{Gyr}$ model and lower limit is determined by constant SFR model such that the model with $z_f = 3$ reproduces the local color range. Even if formation redshift is replaced with $z_f = 5$, predicted color range at $0.5 < z < 2.0$ shows little change. Most disk-dominated galaxies at $z > 1.5$ seem to be roughly consistent with the model. In the model such as $\tau = 5\text{Gyr}$ or constant SFR, these blue rest $U - V$ colors correspond to the age of $\lesssim 2\text{Gyr}$. Although these estimated age can easily change for different star formation history or taking into account of dust extinction, the clear difference of rest $U - V$ color distribution between $z < 1.5$ and $z > 1.5$ seems to reflect that the star formation activity of disk galaxies is stronger at $z > 1.5$ and their stellar age is rather younger.

Regarding the number density of late-type galaxies at $z > 1$, Rodighiero et al.(2000) previously investigated the ground-based K -selected ($K \gtrsim 20.5$) late-type galaxies in the HDF-N selected by light profile fitting, and found the deficit of late-type galaxies at $z > 1.4$. On the other hand, in our $M_V < -20$ sample, where the corresponding limiting magnitude is ~ 1.5 mag fainter than that in Rodighiero et al.(2000) at $z \sim 1.5$, the decrease of the comoving number density of disk-dominated galaxies is only marginal, considering the uncertainty of the photometric redshift technique (Section 3.1, Table 4). If we limit the sample to $M_V < -21.5$, however, we indeed see few disk-dominated galaxies at $z > 1.5$, and therefore the disk-dominated galaxies in our sample have relatively faint ($M_V > -21$) rest V -band luminosity distribution at $z > 1.5$ (Figure 13b). The apparent inconsistency may be due to the luminosity-dependent evolution of the galaxies.

These bluer rest $U - V$ color and fainter V -band luminosity distributions of disk-dominated galaxies at $z > 1.5$ suggest that we see these galaxies at very young stage near the formation epoch.

4.2.3. *Disk Galaxies with Red U-V Color*

At $z < 1.5$, Rodighiero et al.(2000) also pointed out that there are two kinds of population, red and blue in their late-type galaxy sample. In our $M_V < -20$ sample, the relatively red disk-dominated galaxies exist at $z < 1.5$, too.

The colors of rest $U - V \sim 0.8$ of these red galaxies are significantly redder than the prediction of the $\tau = 7$ or 5 Gyr model with $z_f = 3$ or 5 mentioned above. In these star formation history model, these colors correspond to ~ 10 Gyr old at $0.5 < z < 1.5$, which is difficult to be considered in our assumed cosmology. Probably, their red $U - V$ colors are due to less on-going star formation activity or stronger dust extinction effect. As mentioned in Rodighiero et al.(2000), it is difficult to discriminate these two effects and determine the mean age and the dust extinction, respectively with only UV-NIR photometry.

In Figure 6c, we can see the montage of these red disk-dominated galaxies. These galaxies show relatively red color all over the image, therefore if the dust extinction causes their redness, the dust distributes over the whole galaxy.

4.3. *Irregular galaxies*

The relatively bright irregular galaxies in the HDF-N shows the similar comoving number density (Figure 9) with disk-dominated galaxies at $z > 0.5$, which is much larger than that expected from local luminosity function. This rapid increase of the irregular galaxies at $0.5 < z < 1.0$ is consistent with several previous studies (e.g., Brinchmann et al. 1998, Abraham et al. 1996).

The rest-frame $U - V$ color distribution of the irregular galaxies is also similar to or slightly bluer than that of the disk-dominated galaxies, and at $z > 1.5$, all irregular galaxies have also $U - V < 0.3$.

Regarding the origin of irregular galaxies, Corbin et al.(2000) investigated the same WFPC2/NICMOS images of the HDF-N as that used in this paper, and suggested that most irregular galaxies are the minor mergers of disk galaxy with smaller companions. If this is real, the similarity of the evolution of the rest $U - V$ color distribution of the disk-dominated galaxies and the irregular galaxies may be expected assuming that the overall color distribution does not change significantly during such a minor merger. In Figure 18, if the sum of the disk-dominated and irregular galaxies is considered, the number density observed over $0.5 < z < 2$ can be explained by the pure luminosity evolution model of exponentially decaying SFR with $\tau = 7$ or 5Gyr which based on the luminosity function of local disk galaxies.

Walker et al.(1996) performed the N-body simulation of such mergers, and found that as the result of these minor mergers, the bulge of the disk-dominated galaxy is enlarged and the galaxy become slightly earlier-type spiral galaxy. The red disk-dominated galaxies at $z < 1.5$ may be the galaxies whose star

formation activity is suppressed as a result of gas consumption due to starburst or/and gas stripping in these minor mergers.

Also, these red disk-dominated galaxies may be the progenitors of the red irregular galaxies at $z < 1.5$. In this scenario, the fact that at $z > 1.5$, there is no red disk-dominated or irregular galaxy may suggest that at $z > 1.5$, there is no sufficient time when the irregular galaxies due to the minor merger of (initial, pre-merger) blue disk-dominated galaxies relax dynamically and return to (earlier and redder) disk-dominated galaxies. In Walker et al's simulation, it takes about 1.5-2 Gyr since merger started that the disk galaxy with stellar mass of $5.6 \times 10^{10} M_{\odot}$ in minor merger recovers the symmetric surface brightness distribution. If starbursts occur in minor merger, the population formed in these bursts may have relatively red color, such a time after the bursts.

On the other hand, at $z < 1.0$, if these minor merger rate declines rapidly forward $z = 0$, the rapid decrease of the number density of irregular galaxies may be able to be explained. Further, if these minor merger occur in bulge-dominated galaxies at $z < 1$, the wide distribution of the rest $U - V$ color of these galaxies may also be expected in this scenario.

5. Conclusion: When the Hubble sequence appeared ?

In order to understand the formation and evolution of the Hubble sequence, using the HST WFPC2/NICMOS archival data of the Hubble Deep Field North, we constructed the volume-limited sample of $M_V < -20$ galaxies to $z = 2$, and investigated the evolution of the distribution of morphology, luminosity, color of the $M_V < -20$ galaxies.

At $z < 1$, as various studies have showed, the bright irregular galaxies increase rapidly from $z = 0$ to intermediate redshift, while the observed number of the bright early-type and disk galaxies is consistent with mild luminosity evolution with constant number density to $z = 1$. Although their stellar population is younger, at least normal (non-irregular) galaxy portion of Hubble sequence have already formed at $z \sim 1$ in the form such as seen in the present universe.

At $1 < z < 1.5$, the number density of early-type galaxies decreases significantly, even if considering the uncertainty of the photometric redshift. At least for $H_0 = 70 \text{ km s}^{-1} \text{ Mpc}^{-1}$, $\Omega_0 = 0.3$ $\Omega_{\Lambda} = 0.7$ cosmology, the observed number of early-type galaxies at $z > 1$ is deficit relative to the prediction of the pure luminosity evolution model calculated from the local luminosity function. Since that of disk-dominated and irregular galaxies does not show significant evolution, the overall number density of $M_V < -20$ galaxies decrease. Although there is the uncertainty of the effect of the dust extinction on our sample selection, some of the $M_V < -20$ galaxies seem to have formed at these epoch. Similarly, the morphological fraction changes at these redshifts. It indicates that the epoch of the formation of morphology is different between the broad morphological categories, and most early-type galaxies with $L < L^* + 1$ seem to form their appearance as E or S0 at later epoch than similarly bright disk galaxies.

On the other hands, at $1.5 < z < 2.0$, the distribution of rest-frame color of disk galaxies is rather bluer than that at $z = 0$, and it suggests that these galaxies are very young. Since the number density evolution of these galaxies is unclear until the spectroscopic redshifts are obtained by the observation with large telescope, we cannot tell what fraction of disk galaxies forms at $1 < z < 2$, but their formation epoch do not seems to be so much earlier.

These strong evolution at $1.0 < z < 2.0$ suggests that Hubble sequence seen in the present universe as *morphological sequence* is formed at these epoch, although the formation epoch of each galaxy or its stellar population may be still earlier and wide-spread. Regarding the rest $U - V$ color, at $z > 1.5$, Hubble sequence seems to be rather degenerate in blue range, although the marginal trend that the later-type galaxies have bluer colors remains (Figure 19). Considering the HDF-N is at most 4 arcmin^2 , these results are to be confirmed with much larger sample.

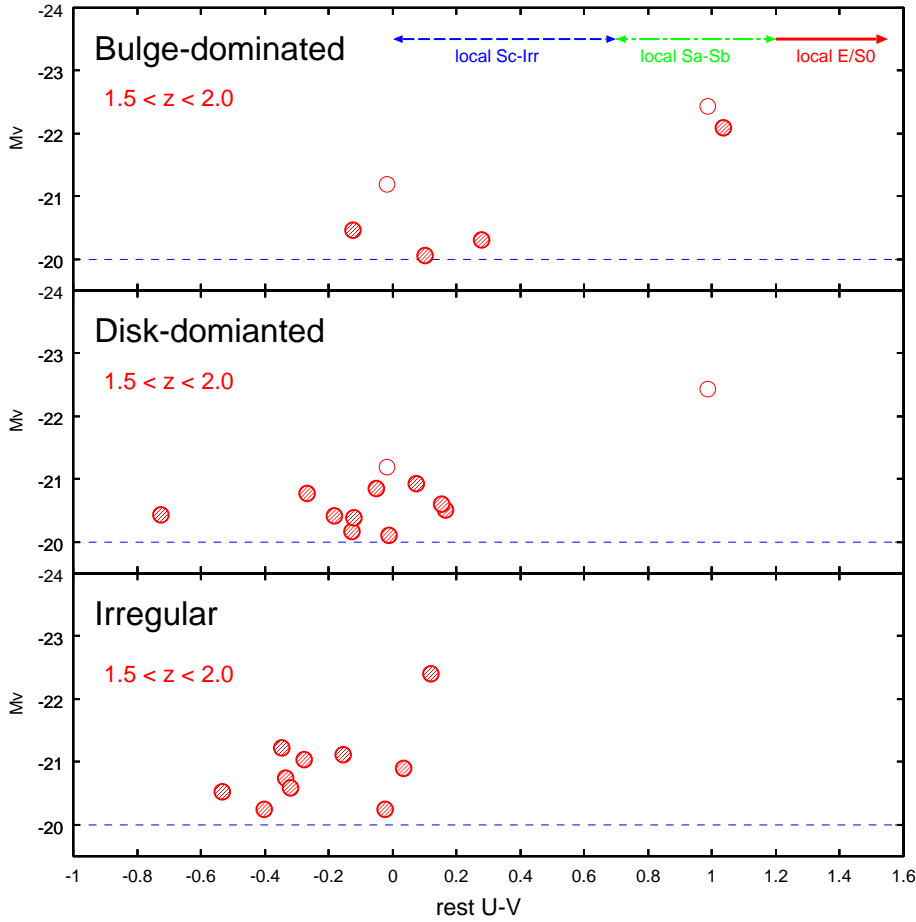


Fig. 19.. Similar with Figure 13 for the $M_V < -20$ galaxies at $1.5 < z < 2.0$ of each morphology. The shaded symbols in each row show bulge-dominated, disk-dominated, irregular galaxies, respectively. The open symbols in top and middle row represent intermediate ones.

Table 1.. Condition of C and A indices for morphological classification

condition	morphology	observed number
$ C_{\text{obs}} - C_{\text{dev}} < \sigma_{\text{dev}} \ \& \ C_{\text{obs}} - C_{\text{exp}} < \sigma_{\text{exp}}$	cannot classify	3
$C_{\text{obs}} > C_{\text{dev}} + 3\sigma_{\text{dev}} \ \& \ C_{\text{obs}} > C_{\text{exp}} + \sigma_{\text{exp}}$	compact	0
$C_{\text{dev}} - \sigma_{\text{dev}} < C_{\text{obs}} < C_{\text{dev}} + 2\sigma_{\text{dev}}$ $\ \& \ C_{\text{obs}} > C_{\text{exp}} + \sigma_{\text{exp}}$ or	bulge-dominated	19
$C_{\text{exp}} + \sigma_{\text{exp}} < C_{\text{obs}} < C_{\text{dev}} - \sigma_{\text{dev}}$ $\ \& \ (C_{\text{obs}} - C_{\text{exp}})/\sigma_{\text{exp}} > 2.5 \times (C_{\text{dev}} - C_{\text{obs}})/\sigma_{\text{dev}}$		
$C_{\text{exp}} + \sigma_{\text{exp}} < C_{\text{obs}} < C_{\text{dev}} - \sigma_{\text{dev}}$ $\ \& \ (C_{\text{obs}} - C_{\text{exp}})/\sigma_{\text{exp}} > 0.4 \times (C_{\text{dev}} - C_{\text{obs}})/\sigma_{\text{dev}}$ $\ \& \ (C_{\text{obs}} - C_{\text{exp}})/\sigma_{\text{exp}} < 2.5 \times (C_{\text{dev}} - C_{\text{obs}})/\sigma_{\text{dev}}$	intermediate	13
$C_{\text{exp}} - 2\sigma_{\text{dev}} < C_{\text{obs}} < C_{\text{exp}} + \sigma_{\text{dev}}$ $\ \& \ C_{\text{obs}} < C_{\text{dev}} - \sigma_{\text{dev}}$ or	disk-dominated	32
$C_{\text{exp}} + \sigma_{\text{exp}} < C_{\text{obs}} < C_{\text{dev}} - \sigma_{\text{dev}}$ $\ \& \ (C_{\text{obs}} - C_{\text{exp}})/\sigma_{\text{exp}} < 0.4 \times (C_{\text{dev}} - C_{\text{obs}})/\sigma_{\text{dev}}$		
$C_{\text{obs}} < C_{\text{exp}} - 3\sigma_{\text{exp}} \ \& \ C_{\text{obs}} < C_{\text{dev}} - \sigma_{\text{dev}}$ or	irregular	27
$A_{\text{obs}} > 0.12 \ \& \ A_{\text{obs}} > A_{\text{art}} + 2\sigma_{\text{art}}$		

Table 2.. I_{814} vs J_{110} -band classification for $0.3 < z < 0.8$

I_{814} -band	J_{110} -band			
	bulge-dominated	intermediate	disk-dominated	irregular
bulge-dominated	4	2	2	0
intermediate	0	2	2	0
disk-dominated	1	0	2	0
irregular	1	0	0	4

Table 3.. J_{110} vs H_{160} -band classification for $0.7 < z < 1.3$

J_{110} -band	H_{160} -band			
	bulge-dominated	intermediate	disk-dominated	irregular
bulge-dominated	6	3	2	0
intermediate	0	4	2	0
disk-dominated	0	3	5	0
irregular	1	1	2	8

Abraham R. G. 1999, Ap&SS, 269, 323

Abraham R. G., van den Berg S., Glazebrook K., Ellis R. S., Santiago B. X., Surma P., Griffiths R. E. 1996, ApJS, 107, 1

Adelberger K. L., Steidel C. C., Giavalisco M., Dickinson M., Pettini M., Kellogg M. 1998, ApJ, 505, 18

Bershady M. A., Jangren A., Conselice C. J. 2000, AJ, 119, 2645

Bertin E., Arnouts S. 1996, A&AS, 117, 393

Bingelli B., Sandage A., Tammann G.A. 1988, ARA&A, 26, 509

Bolzonella M., Miralles J.-M., Pelló R. 2000, A&A, 363, 476

Table 4.. Number of galaxies in each redshift bin and possible escaped and included number for the secondary peak redshift

redshift	bulge-dominated	intermediate	disk-dominated	irregular	cannot classify
0-0.5	4 ± 0	2 ± 0	2_{-0}^{+1}	2 ± 0	0 ± 0
0.5-1.0	13 ± 0	5_{-0}^{+1}	12_{-1}^{+0}	11 ± 0	0 ± 0
1.0-1.5	3 ± 0	6_{-1}^{+0}	9_{-1}^{+3}	5 ± 0	0_{-0}^{+1}
1.5-2.0	4_{-2}^{+1}	2 ± 0	10_{-9}^{+3}	10_{-6}^{+6}	3_{-2}^{+0}

Brinchmann J., Abraham G., Schade D., Tresse L., Ellis R. S., Lilly S., Le Fevre O., Glazebrook K., Hammer F., Colless M., Crampton D., Broadhurst T. 1998, ApJ, 499, 112

Bruzual A. G., Charlot S. 1993, ApJ, 405, 538

Buta R. 1992a, in Morphological and Physical Classification of Galaxies, ed Longo G., Capaccioli M., Busarello, G.(Kluwer, Dordrecht) page1

Buta R. 1992b, in Physics of Nearby Galaxies, ed Thuan T. X., Balkowski C., Van J. T. T.(Frontiers, Gif-sur-Yvette) page3

Calzetti D., Armus L., Bohlin R. C., Kinney A. L., Koornneef J., Storchi-Bergmann T. 2000, ApJ, 533, 682

Cohen J., Hogg D. W., Blandford R., Cowie L. L., Hu E., Songaila A., Shopbell P., Richberg K. 2000, ApJ, 538, 29

Coleman G. D., Wu C.-C., Weedman D. W. 1980, ApJS, 43, 393

Conselice C. J., Bershadsky M. A., Jangren A. 2000, ApJ, 529, 886

Corbin M. R., Urban A., Stobie E., Thompson R. I., Schneider G. 2001, AJ, in press, *astro-ph/0012192*

de Vaucouleurs G. 1959, in Handbuch der Physik, Vol. 53, ed Flugge, S. (Springer-Verlag, Berlin) page275

Dickinson M. 1998, in The Hubble Deep Field, ed Lavio M., Fall S. M., Madu P.(Cambridge Univ. Press, Cambridge) page219

- Dickinson M. 2000a, Philosophical Transactions of the Royal Society of London, Series A, Vol. 358, no. 1772, page2001
- Dickinson M. 2000b, in Building Galaxies:From the Primordial Universe to the Present, ed Hammer F., Thuan T.X., Cayatte V., Guiderdoni B., Trinh Than Van J.(Ed. Frontieres, Paris) page257
- Dickinson M., Hanley C., Elston R., Eisenhardt P. R., Stanford S. A., Adelberget K. L., Shapley A., Steidel C. C., Papovich C., Szalay A. S., Bershadly M. A., Conselice C. J., Ferguson H C., Fruchter A. S. 2000, ApJ 531, 624
- Fernandez-Soto A., Lanzetta K. M., Yahil A. 1999, ApJ, 513, 34
- Franceschini A., Silva L., Fasano G., Granato L., Bressan A., Arnouts S., Danese L. 1998, ApJ, 506, 600
- Haines C. P., Clowes R. G., Campusano L. E., Adamson A. J. 2001, MNRAS in press, *astro-ph/0011415*
- Hubble E. 1926, ApJ, 64, 321
- Hubble E. 1936, The Realm of the Nebulae (Yale Univ. Press, New Haven)
- Huchra J. P. 1977, ApJ, 217, 928
- Kajisawa M. et al. 2000 PASJ, 52, 61
- Kennicutt R. C. 1983, ApJ, 272, 54
- Lilly S., Schade D., Ellis R., Le Fevre O., Brinchmann J., Tresse L., Abraham R., Hammer F., Crampton D., Colles M., Glazebrook K., Mallen-Ornelas G., Broadhurst T. 1998, ApJ, 500, 75
- Lowenthal J. D., Koo D. C., Guzman R., Gallego J., Phillips A. C., Faber S. M., Vogt N. P., Illingworth G. D., Gronwall C. 1997, ApJ, 481, 673
- Marzke R. O., Geller M. J., Huchra, J. P., Corwin, H. G. 1994, AJ, 108, 437
- Marzke R. O., da Costa L. N., Pellegrini P. S., Willmer C. N. A., Geller M. J. 1998, ApJ, 503, 617
- Menanteau F., Ellis R. S., Abraham R. G., Barger A. J., Cowie L. L. 1999, MNRAS, 309, 208
- Nakata F., Kajisawa M., Yamada T., Kodama T., Shimasaku K., Tanaka I. 2001 in preparation.
- O'Connell R. W. 1997, in The Ultraviolet Universe at Low and High Redshift: Probing the Progress of Galaxy Evolution, ed Waller H. W.(American Institute of Physics, New York)

page11

- Oke J. B. 1974, *ApJS*, 27, 21
- Roberts M. S., Haynes M. P. 1994, *ARA&A*, 32, 115
- Rodighiero G., Granato G. L., Franceschini A., Fasano G., Silva L. 2000, *A&A* in press, *astro-ph/0010131*
- Rodighiero G., Franceschini A., Fasano G. 2001, *astro-ph/0101262*
- Sandage A. 1975, in *Stars and Stellar Systems, Vol.9*, ed Sandage A., Sandage M., Kristian J.(Univ. Chicago Press, Chicago) page1
- Sandage A., Tammann G. A. 1987, *A Revised Shapley-Ames Catalog of Bright Galaxies* (Carnegie Insitute of Washington, Washington, D.C.)
- Schade D., Lilly S. J., Le Fevre O., Hammer F., Crampton D. 1996, *ApJ*, 464, 79
- Schade D., Lilly S. J., Crampton D., Ellis R. S., Le Fé vre O, Hammer F., Brinchmann J., Abraham R., Colless M., Glazebrook K., Tresse L., Broadhurst T. 1999, *ApJ*, 525, 31
- Steidel C. C., Giavalisco M., Pettini M., Dickinson M., Adelberger K. L. 1996, *ApJ*, 462, L17
- Steidel C. C., Adelberger K. L., Dickinson M., Giavalisco M., Pettini M., Kellogg M. 1998, *ApJ*, 492, 428
- Steidel C. C., Adelberger K. L., Giavalisco M., Dickinson M., Petteni M. 1999, *ApJ*, 519, 1
- Tanaka I., Yamada T., Aragon-Salamanca A., Kodama T., Miyaji T., Ohta K., Arimoto N. 2000, *ApJ*, 528, 128
- van den Bergh S. 1997, *AJ*, 113, 2054
- van den Bergh S., Cohen J. G., Hogg D. W., Blandford R. 2000, *AJ*, 120, 2190
- Vogt N. P., Forbes D. A., Phillips A. C., Gronwall C., Faber S. M., Illingworth G. D., Koo D. C. 1996, *ApJ*, 465, L15
- Vogt N. P., Phillips A. C., Faber S. M., Gallego J., Gronwall C., Guzman R., Illingworth G. D., Koo D. C., Lowenthal J.D. 1997, *ApJ*, 479, L121
- Walker I. R., Mihos J. C., Hernquist L. 1996, *ApJ*, 460, 121
- Zepf S. E. 1997, *Nature*, 390, 377

This figure "fig6a.jpg" is available in "jpg" format from:

<http://arxiv.org/ps/astro-ph/0105118v3>

This figure "fig6b.jpg" is available in "jpg" format from:

<http://arxiv.org/ps/astro-ph/0105118v3>

This figure "fig6c.jpg" is available in "jpg" format from:

<http://arxiv.org/ps/astro-ph/0105118v3>

This figure "fig6d.jpg" is available in "jpg" format from:

<http://arxiv.org/ps/astro-ph/0105118v3>